4. Ghayur, T. *et al.* Caspase-1 processes IFN-gamma-inducing factor and regulates LPS-induced IFN-gamma production. *Nature* **386,** 619–623 (1997).
5. Rathinam, V. a. K., Vanaja, S. K. & Fitzgerald, K. a. Regulation of inflammasome signaling. *Nat. Immunol.* **13,** 333–2 (2012).
6. Ohnishi, H. *et al.* TRAM is involved in IL-18 signaling and functions as a sorting adaptor for MyD88. *PLoS ONE* **7,** e38423 (2012).
7. Adachi, O. *et al.* Targeted disruption of the MyD88 gene results in loss of IL-1- and IL-18-mediated function. *Immunity* **9,** 143–150 (1998).
8. Hoffman, H. M., Mueller, J. L., Broide, D. H., Wanderer, A. A. & Kolodner, R. D. Mutation of a new gene encoding a putative pyrin-like protein causes familial cold autoinflammatory syndrome and Muckle-Wells syndrome. *Nat. Genet.* **29,** 301–305 (2001).
9. Park, H., Bourla, A. B., Kastner, D. L., Colbert, R. a. & Siegel, R. M. Lighting the fires within: the cell biology of autoinflammatory diseases. *Nat. Rev. Immunol.* **12,** 570–580 (2012).
10. Dinarello, C. a., Simon, A. & van der Meer, J. W. M. Treating inflammation by blocking interleukin-1 in a broad spectrum of diseases. *Nat. Rev. Drug Discov.* **11,** 633–652 (2012).
11. Alboni, S., Cervia, D., Sugama, S. & Conti, B. Interleukin 18 in the CNS. *J. Neuroinflamm.* **7,** 9 (2010).
12. Mellins, E. D., Macaubas, C. & Grom, A. A. Pathogenesis of systemic juvenile idiopathic arthritis: some answers, more questions. *Nat. Rev. Rheumatol.* **7,** 416–426 (2011).
13. Hirota, T. *et al.* Genome-wide association study identifies eight new susceptibility loci for atopic dermatitis in the Japanese population. *Nat. Genet.* **44,** 1222–1226 (2012).
14. Dinarello, C. A., Novick, D., Kim, S. & Kaplanski, G. Interleukin-18 and IL-18 binding protein. *Front. Immunol.* **4,** 289 (2013).
15. Romberg, N. *et al.* Mutation of NLRC4 causes a syndrome of enterocolitis and autoinflammation. *Nat. Genet.* **46,** 1135–1139 (2014).
16. Canna, S. W. *et al.* An activating NLRC4 inflammasome mutation causes autoinflammation with recurrent macrophage activation syndrome. *Nat. Genet.* **46,** 1140–1146 (2014).
17. Terada, M. *et al.* Contribution of IL-18 to atopic-dermatitis-like skin inflammation induced by Staphylococcus aureus product in mice. *Proc. Natl Acad. Sci. USA* **103,** 8816–8821 (2006).
18. Brydges, S. D. *et al.* Divergence of IL-1, IL-18, and cell death in NLRP3 inflammasomopathies. *J. Clin. Invest.* **123,** 4695–4705 (2013).
19. Kato, Z. *et al.* The structure and binding mode of interleukin-18. *Nat. Struct. Biol.* **10,** 966–971 (2003).
20. Krumm, B., Meng, X., Li, Y., Xiang, Y. & Deng, J. Structural basis for antagonism of human interleukin 18 by poxvirus interleukin 18-binding protein. *Proc. Natl Acad. Sci. USA* **105,** 20711–20715 (2008).
21. Argiriadi, M. A., Xiang, T., Wu, C., Ghayur, T. & Borhani, D. W. Unusual water-mediated antigenic recognition of the proinflammatory cytokine interleukin-18. *J. Biol. Chem.* **284,** 24478–24489 (2009).
22. Krumm, B., Meng, X., Wang, Z., Xiang, Y. & Deng, J. A unique bivalent binding and inhibition mechanism by the yatapoxvirus interleukin 18 binding protein. *PLoS Pathog.* **8,** e1002876 (2012).
23. Wang, D. *et al.* Structural insights into the assembly and activation of IL-1β with its receptors. *Nat. Immunol.* **11,** 905–911 (2010).
24. Thomas, C., Bazan, J. F. & Garcia, K. C. Structure of the activating IL-1 receptor signaling complex. *Nat. Struct. Mol. Biol.* **19,** 455–457 (2012).
25. Liu, X. *et al.* Structural insights into the interaction of IL-33 with its receptors. *Proc. Natl. Acad. Sci. USA* **110,** 14918–14923 (2013).
26. Vigers, G. P., Anderson, L. J., Caffes, P. & Brandhuber, B. J. Crystal structure of the type-I interleukin-1 receptor complexed with interleukin-1beta. *Nature* **386,** 190–194 (1997).
27. Günther, S. & Sundberg, E. J. Molecular determinants of agonist and antagonist signaling through the IL-36 receptor. *J. Immunol.* **193,** 921–930 (2014).
28. Takahashi, H., Nakanishi, T., Kami, K., Arata, Y. & Shimada, I. A novel NMR method for determining the interfaces of large protein-protein complexes. *Nat. Struct. Biol.* **7,** 220–223 (2000).
29. Garlanda, C., Dinarello, C. a. & Mantovani, A. The interleukin-1 family: back to the future. *Immunity* **39,** 1003–1018 (2013).
30. Park, E. Y. *et al.* Human IgG1 expression in silkworm larval hemolymph using BmNPV bacmids and its N-linked glycan structure. *J. Biotechnol.* **139,** 108–114 (2009).
31. Nold, M. F. *et al.* IL-37 is a fundamental inhibitor of innate immunity. *Nat. Immunol.* **11,** 1014–1022 (2010).
32. Kumar, S. *et al.* Interleukin-1F7B (IL-1H4/IL-1F7) is processed by caspase-1 and mature IL-1F7B binds to the IL-18 receptor but does not induce IFN-gamma production. *Cytokine* **18,** 61–71 (2002).
33. Hamasaki, T. *et al.* Human anti-human IL-18 antibody recognizing the IL-18-binding site 3 with IL-18 signaling blocking activity. *J. Biochem.* **138,** 433–442 (2005).
34. Kim, S. H. *et al.* Site-specific mutations in the mature form of human IL-18 with enhanced biological activity and decreased neutralization by IL-18 binding protein. *Proc. Natl Acad. Sci. USA* **98,** 3304–3309 (2001).
35. Kimura, T. *et al.* Purification, crystallization and preliminary X-ray crystallographic analysis of human IL-18 and its extracellular complexes. *Acta Crystallogr. Sect. F, Struct. Biol. Commun.* **70,** 1351–1356 (2014).
36. Motohashi, T., Shimojima, T., Fukagawa, T., Maenaka, K. & Park, E. Y. Efficient large-scale protein production of larvae and pupae of silkworm by Bombyx mori nuclear polyhedrosis virus bacmid system. *Biochem. Biophys. Res. Commun.* **326,** 564–569 (2005).
37. Kajikawa, M. *et al.* Silkworm Baculovirus Expression System for Molecular Medicine. *J. Biotechnol. Biomater.* **S9,** 1–5 (2012).
38. Kabsch, W. Xds.. *Acta Crystallogr. D. Biol. Crystallogr.* **66,** 125–132 (2010).
39. Evans, P. Scaling and assessment of data quality. *Acta Crystallogr. D. Biol. Crystallogr.* **62,** 72–82 (2006).
40. Evans, P. R. An introduction to data reduction: space-group determination, scaling and intensity statistics. *Acta Crystallogr. D. Biol. Crystallogr.* **67,** 282–292 (2011).
41. McCoy, A. J. *et al.* Phaser crystallographic software. *J. Appl. Crystallogr.* **40,** 658–674 (2007).
42. Terwilliger, T. C. Statistical density modification with non-crystallographic symmetry. *Acta Crystallogr. D. Biol. Crystallogr.* **58,** 2082–2086 (2002).
43. Emsley, P. & Cowtan, K. Coot: model-building tools for molecular graphics. *Acta Crystallogr. D. Biol. Crystallogr.* **60,** 2126–2132 (2004).
44. Bricogne, G. *et al.* BUSTER. 2.10.0 Ed., Global Phasing Ltd, UK (2011).
45. Smart, O. S. *et al.* Exploiting structure similarity in refinement: automated NCS and target-structure restraints in BUSTER. *Acta Crystallogr. D. Biol. Crystallogr.* **68,** 368–380 (2012).
46. Otwinowski, Z. & Minor, W. Processing of X-ray diffraction data collected in oscillation mode. *Methods Enzymol.* **276,** 307–326 (1997).
47. Lovell, S. C. *et al.* Structure validation by Calpha geometry: phi,psi and Cbeta deviation. *Proteins* **50,** 437–450 (2003).
48. Joosten, R. P. *et al.* A series of PDB related databases for everyday needs. *Nucleic Acids Res.* **39,** D411–D419 (2011).
49. Delaglio, F. *et al.* NMRPipe: a multidimensional spectral processing system based on UNIX pipes. *J. Biomol. NMR* **6,** 277–293 (1995).
50. Lee, W., Westler, W. M., Bahrami, A., Eghbalnia, H. R. & Markley, J. L. PINE-SPARKY: graphical interface for evaluating automated probabilistic peak assignments in protein NMR spectroscopy. *Bioinformatics* **25,** 2085–2087 (2009).
51. Konarev, P. V., Volkov, V. V., Sokolova, A. V., Koch, M. H. J. & Svergun, D. I. PRIMUS: a Windows PC-based system for small-angle scattering data analysis. *J. Appl. Crystallogr.* **36,** 1277–1282 (2003).
52. Svergun, D. I. Determination of the regularization parameter in indirect-transform methods using perceptual criteria. *J. Appl. Crystallogr.* **25,** 495–503 (1992).
53. Svergun, D. I. Restoring low resolution structure of biological macromolecules from solution scattering using simulated annealing. *Biophys. J.* **76,** 2879–2886 (1999).
54. Volkov, V. V. & Svergun, D. I. Uniqueness of ab initio shape determination in small-angle scattering. *J. Appl. Crystallogr.* **36,** 860–864 (2003).
55. Pettersen, E. F. *et al.* UCSF Chimera-a visualization system for exploratory research and analysis. *J. Comput. Chem.* **25,** 1605–1612 (2004).

Acknowledgements

X-ray data collection was supported by SPring-8 (Harima, Japan), Photon Factory (Tsukuba, Japan), Argonne National Laboratory (Illinois, USA, supported by DE-AC02-06CH11357) and Platform for Drug Discovery, Informatics, and Structural Life Science (Japan). We thank T. Tsunaka (Kyoto University) for the use of his beam time of BL44XU at SPring-8. We also thank T. Fukao, N. Kawamoto, K. Tsuji, M. Yamamoto, S. Ninomiya, T. Yano and K. Kasahara (Gifu University) for their scientific advice or technical help. Affymetrix, Inc. provided discontinued detergents to us. SAXS graphics were prepared using the UCSF Chimera package, which developed by the group at the University of California. (San Francisco, USA, supported by NIGMS P41-GM103311). This work was supported by JSPS KAKENHI Grant Number 22370038 to H.T., Grant-in-Aid for JSPS Fellows to N.T., Health and Labour Science Research Grants for Research on Intractable Diseases from the Ministry of Health, Labour and Welfare to H.O., Health and Labour Science Research Grants for Research from the Ministry of Health, Labour and Welfare to Z.K., Science Research Grant from Eishukai to Z.K, and MEXT KAKENHI Grant Number 21790979 to T.K.

Author contributions

H.T. and Z.K. designed the work; M.S and N.K. supervised the study; N.T. carried out the experimental design, experiments and structural analyses, supported by T.K., K.A., M.A. and H.T.; T.K. prepared the samples for the study, supported by H.O., N.T., K.M. and E.Y.P.; T.K. performed and analysed the SPR experiments; T.Y. performed the cell assays,

supported by H.O. and T.K.; X.Z. performed the SAXS measurements; and N.T., T.K., K.A., H.O., Z.K. and H.T. contributed to writing the manuscripts and preparing the figures.

Additional information

Accession codes: The atomic coordinates and structure factors for IL-18, IL-18/IL-18Rα and IL-18/IL-18Rα/IL-18Rβ have been deposited in the RCSB Protein Data Bank under accession codes 3WO2, 3WO3 and 3WO4, respectively.

Supplementary Information accompanies this paper at http://www.nature.com/naturecommunications

Competing financial interests: The authors declare no competing financial interests.

Reprints and permission information is available online at http://npg.nature.com/reprintsandpermissions/

How to cite this article: Tsutsumi, N. *et al.* The structural basis for receptor recognition of human interleukin-18. *Nat. Commun.* 5:5340 doi: 10.1038/ncomms6340 (2014).

Acta Crystallographica Section F
Structural Biology Communications
ISSN 2053-230X

Purification, crystallization and preliminary X-ray crystallographic analysis of human IL-18 and its extracellular complexes

Takeshi Kimura,[a]‡ Naotaka Tsutsumi,[b]‡ Kyohei Arita,[c] Mariko Ariyoshi,[b,d] Hidenori Ohnishi,[a]* Naomi Kondo,[a,e] Masahiro Shirakawa,[b,f] Zenichiro Kato[a,g] and Hidehito Tochio[b]*

[a]Department of Pediatrics, Graduate School of Medicine, Gifu University, Yanagido 1-1, Gifu 501-1194, Japan, [b]Department of Molecular Engineering, Graduate School of Engineering, Kyoto University, Katsura, Nishikyo-ku, Kyoto 615-8510, Japan, [c]Graduate School of Medical Life Science, Yokohama City University, 1-7-29 Suehiro-cho,Tsurumi-ku, Yokohama, Japan, [d]Institute for Integrated Cell-Material Sciences, Kyoto University, Kyoto 606-8501, Japan, [e]Heisei College of Health Sciences, 180 Kurono, Gifu 501-1131, Japan, [f]Core Research of Evolution Science (CREST), Japan Sciences and Technology Agency, Tokyo 102-0076, Japan, and [g]Biomedical Informatics, Medical Information Sciences Division, The United Graduate School of Drug Discovery and Medical Information Sciences, Gifu University, Gifu 501-1194, Japan

‡ Co-first authors.

Correspondence e-mail: ohnishih@gifu-u.ac.jp, tochio@moleng.kyoto-u.ac.jp

Received 10 June 2014
Accepted 22 July 2014

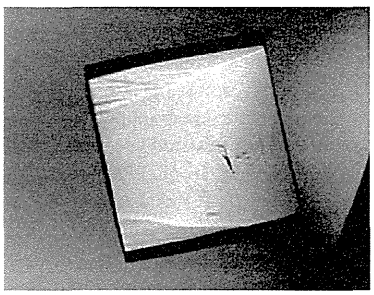

Interleukin-18 (IL-18), a pro-inflammatory cytokine belonging to the interleukin-1 (IL-1) family, is involved in the pathogenesis of autoimmune/autoinflammatory and allergic diseases such as juvenile idiopathic arthritis and bronchial asthma. IL-18 forms a signalling complex with the IL-18 receptor α (IL-18Rα) and β (IL-18Rβ) chains; however, the detailed activation mechanism remains unclear. Here, the IL-18–IL-18Rα binary and IL-18–IL-18Rα–IL-18Rβ ternary complexes were purified and crystallized as well as IL-18 alone. An X-ray diffraction data set for IL-18 was collected to 2.33 Å resolution from a crystal belonging to space group $P2_1$, with unit-cell parameters a = 68.15, b = 79.51, c = 73.46 Å, β = 100.97°. Crystals of both the IL-18 binary and ternary complexes belonging to the orthorhombic space groups $P2_12_12$ and $P2_12_12_1$, respectively, diffracted to 3.10 Å resolution. Unit-cell parameters were determined as a = 135.49, b = 174.81, c = 183.40 Å for the binary complex and a = 72.56, b = 111.56, c = 134.57 Å for the ternary complex.

1. Introduction

IL-18 is a pro-inflammatory cytokine that was first identified as an interferon-γ (IFN-γ)-inducing factor in the sera of endotoxin-injected mice (Okamura *et al.*, 1995). IL-18 not only plays an important role in host defence against microorganisms, but also contributes to the pathogenesis of autoimmune/autoinflammatory and allergic diseases (Nakanishi *et al.*, 2010) such as juvenile idiopathic arthritis (Lotito *et al.*, 2007), familial Mediterranean fever (Simsek *et al.*, 2007), cryopyrin-associated periodic syndrome (Ohnishi *et al.*, 2012), bronchial asthma (Tanaka *et al.*, 2001) and atopic dermatitis (Ohnishi *et al.*, 2003). IL-18 is expressed by various cell types including macrophages, keratinocytes and osteoblasts (Lorey *et al.*, 2004) and belongs to the IL-1 superfamily, sharing structural and functional properties with IL-1β. IL-18 also shares the same signalling cascade with IL-1β. The inflammatory cytokines or stimulants for Toll-like receptors activate intracellular NOD-like receptors such as NLRP3. Activated NLRP3 recruits adaptor protein ASC and caspase-1 precursor (pro-caspase-1); collectively, these proteins form a complex referred to as the inflammasome (Srinivasula *et al.*, 2002). Formation of the inflammasome leads to autocatalytic cleavage of pro-caspase-1, and activated caspase-1 subsequently maturates the IL-18 precursor, which is then secreted outside the cell. To initiate IL-18 intracellular signalling, mature IL-18 is required for the assembly of IL-18Rα and IL-18Rβ. First IL-18 binds to IL-18Rα at the plasma membrane, and then IL-18Rβ binds to the IL-18–IL-18Rα heterodimeric complex (Kato *et al.*, 2003). Assembly of the extracellular region juxtaposes the intracellular Toll-IL-1 receptor (TIR) domains of IL-18Rα and IL-18Rβ, which recruit the adapter molecule MyD88 and sequentially activate IRAKs, TRAF6 and finally NF-κB (O'Neill & Greene, 1998). This signalling cascade then up-regulates the expression of inflammatory cytokines such as IFN-γ. Increased serum levels of IL-18 are frequently correlated with the severity of the autoimmune and autoinflammatory diseases described above. Because of its critical

Table 1
Macromolecule-production information.

Amino acids shown in bold were removed after protease cleavage.

Gene	IL-18	IL-18Rα	IL-18Rβ
Source organism	*Homo sapiens*	*Homo sapiens*	*Homo sapiens*
DNA source	Blood	Blood	Blood
Forward primer	GGATCCATCGAAGGTCGTTACTTTGGCAAGCTTGAATC	GAATTCATGCCCATGTTAAGCGCTATTGTTTTATATGTG-CTTTTGGCGGCGGCGGCGCATTCTGCCTTTGCGGAA-TCTTGTACTTCACGTCCCC	GAATTCATGCCCATGTTAAGCGCTATTGTTTTATATGTG-CTTTTGGCGGCGGCGGCGCATTCTGCCTTTGCGGAG-CGAATTAAAGGATTTAATATTTCAGGTTG
Reverse primer	GAATTCGCTAGTCTTCGTTTTGAACAGTGAAC	GCGGCCGCCTATCTTGTGAAGACGTGGCC	GCGGCCGCTCATCTCTTTTCTTTCAGTTGGACGGAC
Cloning vector	pGEM-T vector	pGEM-T vector	pGEM-T vector
Expression vector	pGEX-4T1	pFastBac1	pFastBac1
Expression host	*E. coli* BL21(DE3)	Sf9 insect cells	Sf9 insect cells
Complete amino-acid sequence of the construct produced	**MSPILGYWKIKGLVQPTRLLLEYLEEKYEEHLYERDEGD-**KWRNKKFELGLEFPNLPYYIDGDVKLTQSMAIIRYI-ADKHNMLGGCPKERAEISMLEGAVLDIRYGVSRIAY-SKDFETLKVDFLSKLPEMLKMFEDRLCHKTYLNGDH-VTHPDFMLYDALDVVLYMDPMCLDAFPKLVCFKKRI-EAIPQIDKYLKSSKYIAWPLQGWQATFGGGDHPPKS-DLVPRGSIEGRYFGKLESKLSVIRNLNDQVLFIDQG-YFGKLESKLSVIRNLNDQVLFIDQGNRPLFEDMTDS-DCRDNAPRTIFIISMYKDSQPRGMAVTISVKCEKIS-TLSCENKIISFKEMNPPDNIKDTKSDIIFFQRSVPG-HDNKMQFESSSYEGYFLACEKERDLFKLILKKEDEL-GDRSIMFTVQNED	HHHHHHHHLEVLFQGPSCTSRPHITVVEGEPFYLKHCSC-GPSCTSRPHITVVEGEPFYLKHCSCSLAHEIETTTK-SWYKSSGSQEHVELNPRSSSRIALHDCVLEFWPVEL-NDTGSYFFQMKNYTQKWKLNVIRRNKHSCFTERQVT-SKIVEVKKFFQITCENSYYQTLVNSTSLYKNCKKLL-LENNKNPTIKKNAEFEDQGYYSCVHFLHHNGKLFNI-TKTFNITIVEDRSNIVPVLLGPKLNHVAVELGKNVR-LNCSALLNEEDVIYWMFGEENGSDPNIHEEKEMRIM-TPEGKWHASKVLRIENIGESNLNVLYNCTVASTGGT-DTKSFILVRKAD	HHHHHHHHLEVLFQGPFNISGCSTKKLLWTYSTRSEEEF-GPFNISGCSTKKLLWTYSTRSEEEFVLFCDLPEPQK-SHFCHRNRLSPKQVPEHLPFMGSNDLSDVQWYQQPS-NGDPLEDIRKSYPHIIQDKCTLHFLTPGVNNSGSYI-CRPKMIKSPYDVACCVKMILEVKPQTNASCEYSASH-KQDLLLGSTGSISCPSLSCQSDAQSPAVTWYKNGKL-LSVERSNRIVVDEVYDYHQGTYVCDYTQSDTVSSWT-VRAVVQVRTIVGDTKLKPDILDPVEDTLEVELGKPL-TISCKARFGFERVFNPVIKWYIKDSDLEWEVSVPEA-KSIKSTLKDEIIERNIILEKVTQRDLRRKFVCFVQN-SIGNTTQSVQLKEKR

role in mediating inflammatory immune responses *in vivo*, IL-18 is normally regulated *via* the naturally occurring IL-18-binding protein (IL-18BP). IL-18BP specifically binds to IL-18 with high affinity, with a dissociation constant of 0.4 n*M*, and prevents IL-18 recognition of IL-18Rα (Dinarello *et al.*, 2013), which is functionally analogous to inhibition of IL-1β signalling by the IL-1β decoy receptor (IL-1RII). Indeed, the potent ability of IL-18 to mediate severe chronic disease has attracted a great deal of interest in the development of new therapeutic reagents that target the IL-18 signalling pathway. However, the structural basis of the IL-18 signalling complex, which can dramatically promote the rational design of IL-18 inhibitory drugs, remains unclear. To this end, we purified and crystallized the IL-18–IL-18Rα binary and IL-18–IL-18Rα–IL-18Rβ ternary complexes as well as the IL-18 monomer; here, we report the preliminary X-ray analysis of each protein.

2. Materials and methods

2.1. Cloning, expression and purification of IL-18, IL-18Rα and IL-18Rβ

IL-18 was overproduced with minor modification of the induction conditions and purified as described previously (Li *et al.*, 2003). Briefly, mature human IL-18 (residues 1–157) fused with a factor Xa recognition site at the N-terminus was cloned into the pGEX 4T-1 vector (GE Healthcare, Little Chalfont, England). IL-18 was expressed as a glutathione *S*-transferase (GST) fusion protein in *Escherichia coli* strain BL21(DE3) with 0.05 m*M* isopropyl β-D-1-thiogalactopyranoside. After GST affinity chromatography and removal of the GST tag by digestion with factor Xa, IL-18 was purified by gel-filtration column chromatography. The extracellular domains of human IL-18Rα (NM_003855, residues 20–329) or IL-18Rβ (NM_003853, residues 15–356) were each cloned separately into the pFastBac1 baculovirus transfer vector (Invitrogen, Carlsbad, California, USA) with an N-terminal signal peptide sequence for Sf9 insect cells, an 8×His tag and a human rhinovirus (HRV) 3C protease cleavage site. Firstly, the coding sequence of each extracellular domain was amplified by PCR with primers containing the signal peptide sequence (Table 1) and then ligated into the pFastBac1 vector between *Eco*RI and *Not*I restriction sites. Secondly, a DNA oligo (48 bp) encoding an 8×His tag and an HRV 3C cleavage site was phosphorylated by T4 kinase (Toyobo, Osaka, Japan) and inserted into the linearized transfer vectors, which were prepared by PCR, using the blunt-end ligation method. Consequently, an 8×His tag cleavable by HRV 3C protease was inserted before the coding sequences. IL-18Rα and IL-18Rβ were expressed using the same protocol. The modified transfer vector was introduced into *E. coli* DH10Bac (Invitrogen) to generate bacmid DNA, which was transfected into Sf9 cells to generate recombinant baculovirus. The baculovirus was then amplified in two cycles. For IL-18 receptor production, Sf9 cell cultures at a density of 2×10^6 cells ml^{-1} were infected with the recombinant baculovirus at a multiplicity of infection (m.o.i.) of 0.1 plaque-forming units (pfu) per cell. Baculovirus-infected Sf9 culture media were harvested after 72 h by centrifugation. The IL-18 receptors were each purified separately using the same chromatographic steps. The receptor secreted from Sf9 cells was collected with ion-exchange columns from the culture media, most impurities were removed using Q Sepharose (GE Healthcare) and the IL-18 receptor in the flowthrough was captured by SP Sepharose (GE Healthcare). After an extensive washing step with 50 m*M* sodium phosphate buffer pH 6.0 containing 50 m*M* sodium chloride, the IL-18 receptor was eluted from an SP Sepharose column with 50 m*M* sodium phosphate buffer pH 6.0 containing 500 m*M* sodium chloride. The pH of the eluate was then adjusted to 7.4 with sodium hydroxide solution and the 8×His-tagged proteins were purified by Ni–NTA agarose (Qiagen, Venlo, Netherlands) chromatography with elution buffer containing an linear gradient of imidazole concentration from 150 to 250 m*M*. After digestion of the N-terminal 8×His tag with HRV 3C protease, the receptor was further purified by size-exclusion chromatography on an Superdex 75 26/60 column (GE Healthcare) with 20 m*M* sodium phosphate buffer pH 7.0 containing 150 m*M* sodium chloride and 0.1 m*M* ethylenediaminetetraacetic acid; the HRV 3C protease was removed in this step.

To obtain the IL-18–IL-18Rα binary and IL-18–IL-18Rα–IL-18Rβ ternary complexes, IL-18, IL-18Rα and IL-18Rβ were mixed in equimolar ratios and purified by gel-filtration chromatography on a Superdex 200 16/60 column with the same buffer as that used in the previous gel-filtration step. Protein elution was monitored at a wavelength of 280 nm. Moreover, we assessed the molecular weights of each protein or protein complex using analytical gel-filtration

Table 2
Crystallization.

Sample	IL-18	IL-18–IL-18Rα	IL-18–IL-18Rα–IL-18Rβ
Method	Vapour diffusion	Vapour diffusion	Vapour diffusion
Plate type	Hanging drop	Hanging drop	Sitting drop
Temperature (K)	277	293	277
Protein concentration (mg ml^{-1})	7	9	10
Buffer composition of protein solution	5 m*M* HEPES–Na pH 7.0, 10 m*M* NaCl	5 m*M* HEPES–Na pH 7.0, 10 m*M* NaCl	5 m*M* HEPES–Na pH 7.0, 10 m*M* NaCl
Composition of reservoir solution	2.5 *M* ammonium sulfate, 100 m*M* bis-tris–HCl pH 7.0	35% PEE 797, 350 m*M* ammonium sulfate, 50 m*M* CAPS pH 9.0 with or without 450 m*M* NDSB-201	18% PEG 4000, 200 m*M* $MgCl_2$, 40 m*M* $[Co(NH_3)_6]Cl_3$, 100 m*M* Tris–HCl pH 7.4
Additive solution	0.25%(*w*/*v*) CHAPS	50 m*M* LysoFos Choline 10 or LysoFos Choline Ether 10	None
Volume ratio of drop† (µl)	0.4:0.4:0.2	With NDSB-201, 1.0:1.0:0; without NDSB-201, 1.0:1.0:0.5	1.0:1.0

† The mixed volume ratio of protein solution:reservoir solution:additive solution.

Table 3
Data collection and processing.

Values in parentheses are for the outer shell.

Molecule	IL-18	IL-18–IL-18Rα	IL-18–IL-18Rα	IL-18–IL-18Rα	IL-18–IL-18Rα–IL-18Rβ
Detergent	CHAPS	NDSB-201	LysoFos Choline Ether 10	LysoFos Choline 10	None
Diffraction source	BL38B1, SPring-8	BL1A, PF	BL5A, PF	BL44XU, SPring-8	BL17A, PF
Wavelength (Å)	1.0000	1.1000	0.9407	0.9000	0.9800
Temperature (K)	100	100	100	100	100
Detector	ADSC Q315	Dectris PILATUS 2M	ADSC Q315	Rayonix MX225HE	ADSC Q270
Crystal-to-detector distance (mm)	300.0	328.7	319.6	300.0	309.6
Software	*XDS*/*SCALA*	*HKL*-2000	*XDS*/*SCALA*	*XDS*/*SCALA*	*HKL*-2000
Space group	$P2_1$	$P6_222$ or $P6_422$	$P2_12_12$	$P2_12_12$	$P2_12_12_1$
a, *b*, *c* (Å)	68.15, 79.51, 73.46	148.05, 148.05, 226.35	136.09, 175.65, 184.57	135.49, 174.81, 183.40	72.56, 111.56, 134.57
α, β, γ (°)	90.00, 100.97, 90.00	90.00, 90.00, 120.00	90.00, 90.00, 90.00	90.00, 90.00, 90.00	90.00, 90.00, 90.00
Theoretical or estimated MW† (kDa)	18.2	70.0	70.0	70.0	119.5
Molecules in asymmetric unit	4	2	6	6	1
V_M (Å^3 Da^{-1})	2.68	2.56	2.63	2.59	2.28
Resolution range (Å)	45.0–2.33 (2.46–2.33)	42.0–3.90 (4.04–3.90)	47.3–3.30 (3.48–3.30)	43.9–3.10 (3.27–3.10)	50.0–3.10 (3.21–3.10)
Total No. of reflections	121376	144429	989916	296079	202352
No. of unique reflections	32990	13981	66776	79180	20587
Completeness (%)	97.8 (97.1)	100 (99.9)	99.4 (99.1)	99.6 (100)	99.9 (99.3)
Multiplicity	3.8 (3.8)	10.3 (10.4)	14.8 (15.3)	3.7 (3.8)	9.8 (9.2)
$\langle I/\sigma(I)\rangle$	20.5 (3.6)	15.2 (2.1)	20.0 (4.5)	14.9 (2.5)	19.8 (2.9)
$R_{r.i.m.}$ (%)	5.7 (46.1)	15.0 (75.6)	14.2 (84.1)	11.7 (67.8)	12.1 (72.3)

† The molecular weights (MW) of the binary and ternary complexes are estimated from the gel-filtration profile because the receptors have heterogeneous N-linked high-mannose glycans. The values are used for calculation of the Matthews coefficient (V_M).

column chromatography. The three proteins were mixed in all possible combinations and each sample was loaded onto a Superdex 200 10/300 GL column (GE Healthcare). Each sample was isocratically eluted at a flow rate of 0.25 ml min^{-1} in 50 m*M* sodium phosphate pH 7.0, 150 m*M* sodium chloride. The molecular masses were estimated using a calibration curve of gel-filtration standards (Bio-Rad, Hercules, California, USA).

2.2. Crystallization

Before crystallization, the protein samples were dialyzed against 5 m*M* HEPES–Na pH 7.0 containing 10 m*M* sodium chloride. Crystallization screening of IL-18 was conducted using the hanging-drop vapour-diffusion method in 24-well plates. Crystals were obtained using an ammonium sulfate-based screening kit (Hampton Research, McLean, Virginia, USA). Subsequently, the crystallization conditions were optimized by adding detergent: 400 nl of 7.0 mg ml^{-1} protein solution was mixed with 400 nl precipitant solution and 200 nl 0.25%(*w*/*v*) CHAPS (Dojindo, Kumamoto, Japan). This mixture was then equilibrated against 500 µl precipitant solution. Crystallization screening of the binary and ternary complexes was carried out using the sitting-drop vapour-diffusion method in 96-well plates, in which 100 nl protein solution was mixed with 100 nl of each precipitant solution. Crystals of the IL-18–IL-18Rα complex were obtained using a pentaerythritol ethoxylate (15/4 EO/OH, PEE 797)-based screening kit (Jena Bioscience, Jena, Germany), while the IL-18–IL-18Rα–IL-18Rβ ternary complex was crystallized using a polyethylene glycol (PEG) 4000-based screening kit (Jena Bioscience). The crystallization conditions for both complexes were optimized by screening various detergents and additives. Crystallizations with optimized conditions were scaled up using the hanging-drop or sitting-drop vapour-diffusion method with 24-well plates in which 1 µl protein solution and 1 µl precipitant solution were typically mixed with or without 0.5 µl detergent. Crystallization drops of the IL-18–IL-18Rα complex were immediately equilibrated with 500 µl precipitant solution. Crystallization of the IL-18–IL-18Rα–IL-18Rβ complex required a dehydration step prior to vapour diffusion, in which the crystallization drops were air-dried for 6 h at 293 K and subsequently placed over reservoir chambers filled with 200 µl of each precipitant solution. Crystallization plates were incubated under protection from light at 277 K for IL-18 and IL-18–IL-18Rα–IL-18Rβ or 293 K for IL-18–IL-18Rα. The final conditions are summarized in Table 2.

2.3. X-ray diffraction data collection and processing

The crystals from each precipitant solution (including detergents) were flash-cooled in liquid nitrogen with cryoprotectant solutions containing 20%(*w*/*v*) glycerol (IL-18 and IL-18–IL-18Rα–IL-18Rβ)

or 20%(*w*/*v*) glucose (IL-18–IL-18Rα). X-ray diffraction data sets were collected at 100 K using the synchrotron beamlines at SPring-8, Harima, Japan or Photon Factory (PF), Tsukuba, Japan. The intensity data were processed using *XDS* (Kabsch, 2010) and *SCALA* (Evans, 2006) or *HKL*-2000 software (Otwinowski & Minor, 1997). When the *XDS* and *SCALA* software were used, the space group was determined using *POINTLESS* (Evans, 2006). The crystallographic data-collection statistics for IL-18, IL-18–IL-18Rα and IL-18–IL-18Rα–IL-18Rβ are summarized in Table 3. For the IL-18–IL-18Rα crystals, the statistics with three detergents NDSB-201 (Merck, Whitehouse Station, New Jersey, USA), LysoFos Choline Ether 10 (Affymetrix, Santa Clara, California, USA) and LysoFos Choline 10 (Affymetrix) are shown to indicate the improvement in the data quality.

3. Results and discussion

3.1. Reconstitution of the extracellular IL-18 signalling complex

We previously established a bacterial overexpression and purification system for IL-18 (Li *et al.*, 2003). For structural analysis of the IL-18-mediated signalling complexes, we used a baculovirus expression system to obtain sufficient amounts of the IL-18Rα and IL-18Rβ receptors for crystallization experiments. Each receptor expressed from Sf9 cells was purified by three chromatographic steps: ion-exchange, metal-affinity and gel-filtration chromatography using Q and SP Sepharose, Ni–NTA agarose (Figs. 1*a* and 1*b*) and Superdex 75 26/60 (Figs. 1*c* and 1*d*). Finally, ~4 mg IL-18Rα and ~1 mg IL-18Rβ protein with a purity greater than 90% were obtained from 1 l

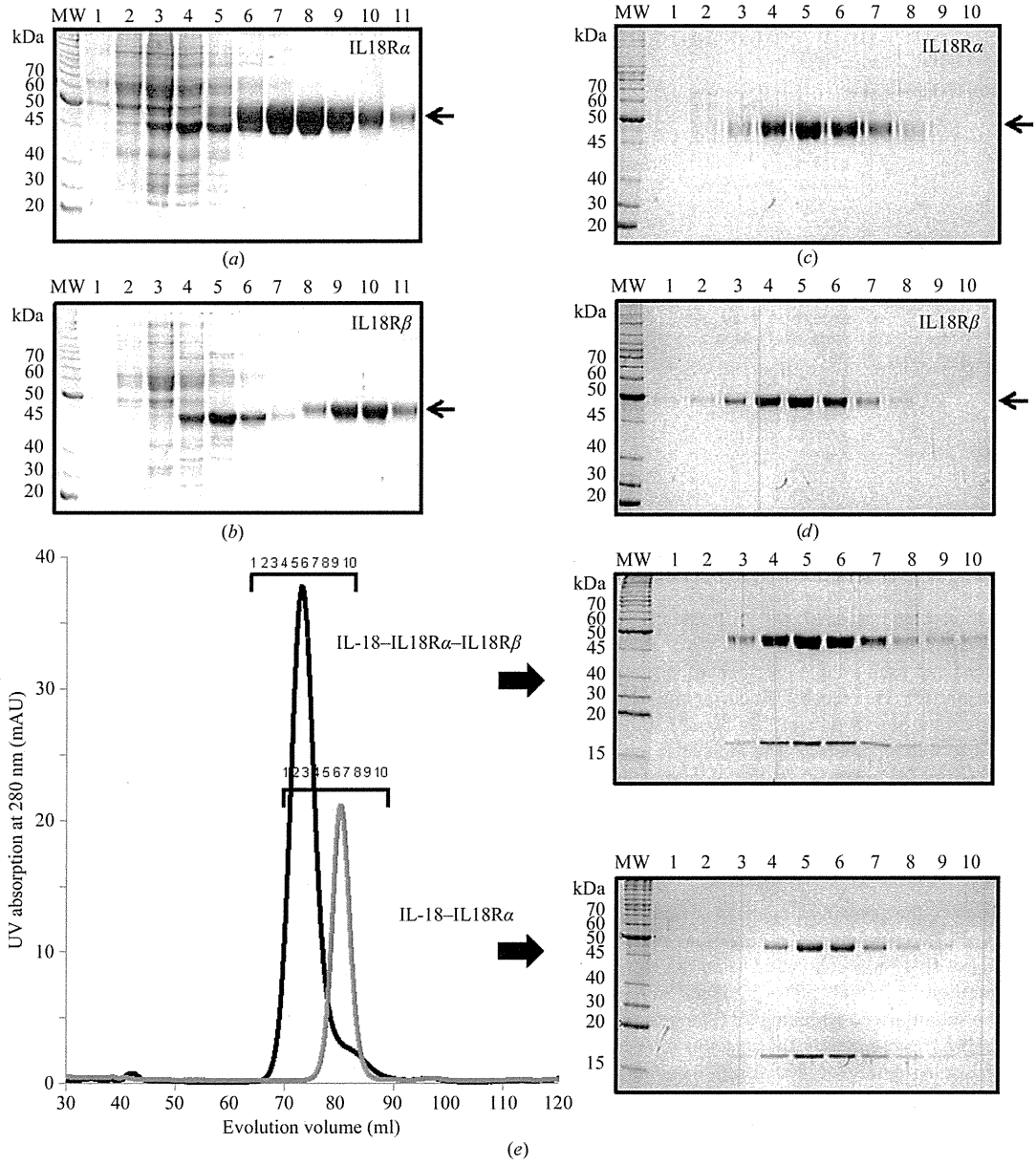

Figure 1
SDS–PAGE analysis of each purification stage. Elution fractions of (*a*) IL-18Rα and (*b*) IL-18Rβ from an Ni–NTA agarose column with an imidazole linear gradient. Peak fractions of (*c*) IL-18Rα and (*d*) IL-18Rβ on size-exclusion chromatography. (*e*) Elution profiles of the IL-18 binary (gray) and IL-18 ternary (black) complexes on size-exclusion chromatography; the peak fractions were analyzed by SDS–PAGE.

Sf9 cell culture (Figs. 1*c* and 1*d*), while ~5 mg of IL-18 was obtained from 1 l *E. coli* culture. To form the binary and ternary complexes, purified IL-18, IL-18Rα and IL-18Rβ were mixed and loaded onto a Superdex 200 16/60 column and each complex was isocratically eluted as a single peak (Fig. 1*e*).

The IL-18 ternary complex was previously reported to assemble in a hierarchical order (Kato *et al.*, 2003). We confirmed this finding and its stoichiometry using analytical gel-filtration column chromatography with purified recombinant proteins. Formation of a ternary complex (MW 119.5 kDa) with 1:1:1 stoichiometry was clearly observed (Fig. 2*a*). In the absence of IL-18Rβ (MW 51.5 kDa), IL-18Rα (MW 61.4 kDa) and IL-18 (MW 18.6 kDa) co-eluted as a complex with an estimated molecular mass of 70.0 kDa, suggesting stable 1:1 complex formation (Fig. 2*a*). In contrast, the IL-18Rβ receptor did not show complex formation with IL-18Rα or IL-18 alone (Figs. 2*b* and 2*c*). Thus, our data clearly demonstrate that the IL-18–IL-18Rα binary complex is required for the binding of IL-18Rβ. Both the IL-18–IL-18Rα and IL-18–IL-18Rα–IL-18Rβ complexes were subjected to crystallization screening.

3.2. Crystallization and preliminary crystallographic analysis

Optimized crystallization conditions are summarized in Table 2. Single crystals of IL-18 with typical dimensions of 200 × 200 × 200 µm (maximum dimensions 300 × 300 × 300 µm) appeared within one week at 277 K (Fig. 3*a*). Crystals of IL-18–IL-18Rα were obtained with various detergents as indicated in Table 2. Spherical moss-like crystals were initially obtained, but three single-crystal forms appeared in the presence of different detergents within a few days at 293 K; these detergents were NDSB-201 (Fig. 3*b*), LysoFos Choline Ether 10 (Fig. 3*c*) and LysoFos Choline 10 (Fig. 3*d*). A single crystal of IL-18–IL-18Rα–IL-18Rβ with dimensions of 50 × 50 × 300 µm appeared within a few weeks at 277 K (Fig. 3*e*).

Crystals of IL-18 diffracted to 2.33 Å resolution and belonged to space group $P2_1$, with unit-cell parameters a = 68.15, b = 79.51, c = 73.46 Å, β = 100.97°. The IL-18–IL-18Rα complex crystals obtained with NDSB-201 or LysoFos Choline Ether 10 diffracted to 3.90 and 3.30 Å resolution, respectively, and a complete data set was collected for each. Of the three crystal forms, the crystal obtained with LysoFos Choline 10 yielded a complete data set at the highest resolution, 3.10 Å, and belonged to space group $P2_12_12$, with unit-cell parameters a = 135.49, b = 174.81, c = 183.40 Å. The crystal of the IL-18–IL-18Rα–IL-18Rβ complex diffracted to 3.10 Å resolution and belonged to space group $P2_12_12_1$, with unit-cell parameters a = 72.56, b = 111.56, c = 134.57 Å. Crystallographic data and X-ray data-collection statistics are summarized in Table 3. Further structural determination is in progress.

X-ray data collection was supported by SPring-8 (Harima, Japan), the Photon Factory (Tsukuba, Japan) and the Platform for Drug Discovery, Informatics and Structural Life Science (Japan). We thank T. Tsunaka (Kyoto University) for his support in the use of beamline

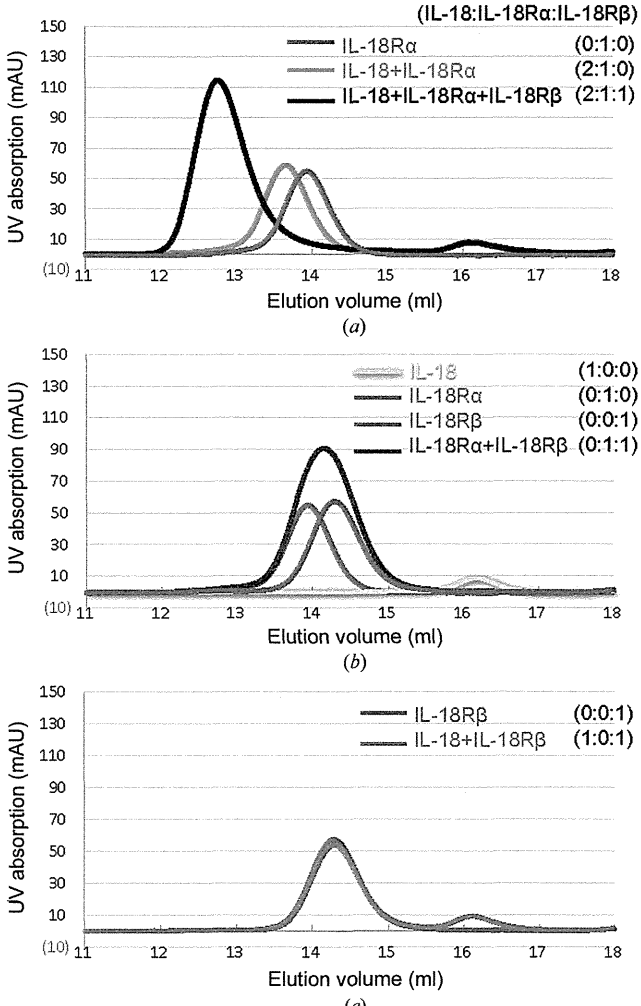

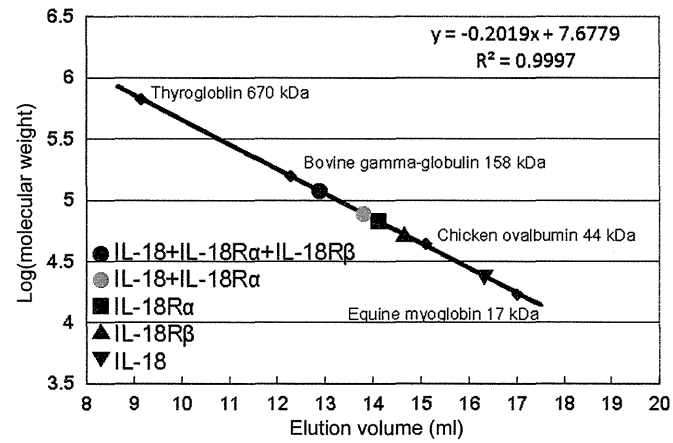

	kDa
IL-18	18.6
IL-18Rα	61.4
IL-18Rβ	51.5
IL-18+IL-18Rα	70.0
IL-18+IL-18Rα+IL-18Rβ	119.5

(*e*)

Figure 2
Gel-filtration profiles for recombinant IL-18, IL-18Rα and IL-18Rβ and their mixtures in all possible combinations. IL-18 and its receptors were mixed at the ratios indicated. (*a*) The typical trace for the binary IL-18–IL-18Rα complex (orange) and ternary IL-18–IL-18Rα–IL-18Rβ complex (black). (*b*) The elution profile for a 1:1 mixture of IL-18Rα and IL-18Rβ (purple) overlaid with that for each receptor alone (red or blue). (*c*) The IL-18 and IL-18Rβ mixture (green) eluted in two separated peaks. (*d*) The elution volumes for IL-18, IL-18Rα, IL-18Rβ and its complexes were plotted against the calibration line. (*e*) A summary of the deduced molecular weights.

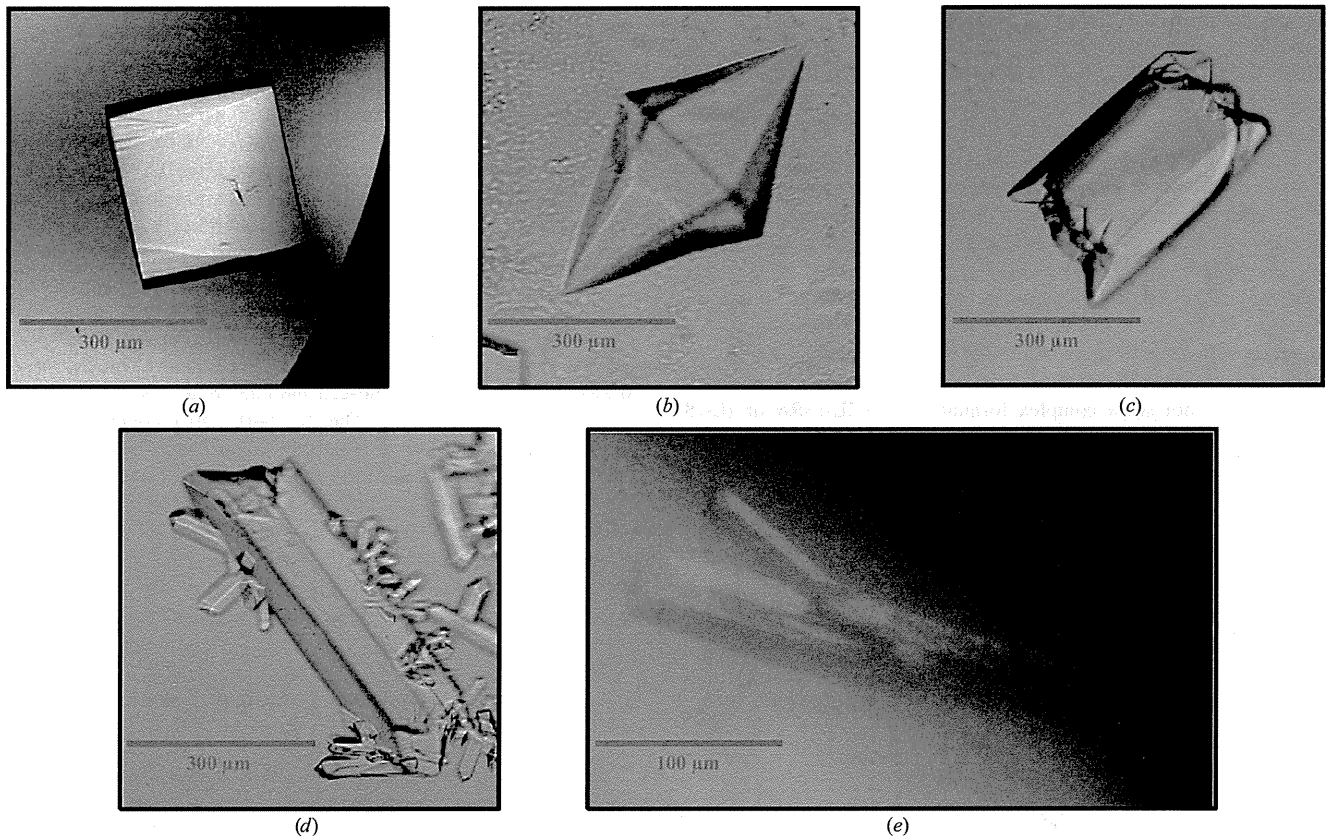

Figure 3
Crystals of IL-18 alone and its extracellular complexes. (*a*) A crystal of IL-18. (*b*) A hexagonal crystal of IL-18–IL-18Rα obtained with NDSB-201. (*c*, *d*) Orthogonal crystals of IL-18–IL-18Rα obtained with (*c*) LysoFos Choline Ether 10 and (*d*) LysoFos Choline 10. (*e*) Crystals of IL-18–IL-18Rα–IL-18Rβ.

BL44XU at SPring-8. We also thank N. Kawamoto, K. Tsuji, M. Yamamoto and K. Kasahara (Gifu University) for their technical assistance. Affymetrix Inc. provided us with discontinued detergents. This work was supported by JSPS KAKENHI Grant Number 22370038 to HT, Grant-in-Aid for JSPS Fellows to NT, and Health and Labour Science Research Grants for Research on Intractable Diseases from the Ministry of Health, Labour and Welfare to HO.

References

Dinarello, C. A., Novick, D., Kim, S. & Kaplanski, G. (2013). *Frontiers Immunol.* **4**, 289.
Evans, P. (2006). *Acta Cryst.* D**62**, 72–82.
Kabsch, W. (2010). *Acta Cryst.* D**66**, 125–132.
Kato, Z., Jee, J., Shikano, H., Mishima, M., Ohki, I., Ohnishi, H., Li, A., Hashimoto, K., Matsukuma, E., Omoya, K., Yamamoto, Y., Yoneda, T., Hara, T., Kondo, N. & Shirakawa, M. (2003). *Nature Struct. Biol.* **10**, 966–971.
Li, A., Kato, Z., Ohnishi, H., Hashimoto, K., Matsukuma, E., Omoya, K., Yamamoto, Y. & Kondo, N. (2003). *Protein Expr. Purif.* **32**, 110–118.
Lorey, S. L., Huang, Y. C. & Sharma, V. (2004). *Clin. Exp. Immunol.* **136**, 456–462.
Lotito, A. P. N., Campa, A., Silva, C. A. A., Kiss, M. H. B. & Mello, S. B. V. (2007). *J. Rheumatol.* **34**, 823–830.
Nakanishi, K., Tsutsui, H. & Yoshimoto, T. (2010). *Allergol. Int.* **59**, 137–141.
Ohnishi, H., Kato, Z., Watanabe, M., Fukutomi, O., Inoue, R., Teramoto, T. & Kondo, N. (2003). *Allergol. Int.* **52**, 123–130.
Ohnishi, H., Teramoto, T., Iwata, H., Kato, Z., Kimura, T., Kubota, K., Nishikomori, R., Kaneko, H., Seishima, M. & Kondo, N. (2012). *J. Clin. Immunol.* **32**, 221–229.
Okamura, H. *et al.* (1995). *Nature (London)*, **378**, 88–91.
O'Neill, L. A. & Greene, C. (1998). *J. Leukoc. Biol.* **63**, 650–657.
Otwinowski, Z. & Minor, W. (1997). *Methods Enzymol.* **276**, 307–326.
Simsek, I., Pay, S., Pekel, A., Dinc, A., Musabak, U., Erdem, H. & Sengul, A. (2007). *Rheumatol. Int.* **27**, 807–811.
Srinivasula, S. M., Poyet, J.-L., Razmara, M., Datta, P., Zhang, Z. & Alnemri, E. S. (2002). *J. Biol. Chem.* **277**, 21119–21122.
Tanaka, H., Miyazaki, N., Oashi, K., Teramoto, S., Shiratori, M., Hashimoto, M., Ohmichi, M. & Abe, S. (2001). *J. Allergy Clin. Immunol.* **107**, 331–336.

ELSEVIER

Brain & Development xxx (2014) xxx–xxx

BRAIN & DEVELOPMENT
Official Journal of the Japanese Society of Child Neurology

www.elsevier.com/locate/braindev

Original article

Trinucleotide insertion in the *SMN2* promoter may not be related to the clinical phenotype of SMA

Nur Imma Fatimah Harahap [a], Atsuko Takeuchi [b], Surini Yusoff [a,c], Koji Tominaga [d], Takeshi Okinaga [e], Yukihiro Kitai [f], Toru Takarada [b], Yuji Kubo [g], Kayoko Saito [g], Nihayatus Sa'adah [a], Dian Kesumapramudya Nurputra [a], Noriyuki Nishimura [a,h], Toshio Saito [i], Hisahide Nishio [a,h,*]

[a] *Department of Community Medicine and Social Healthcare Science, Kobe University Graduate School of Medicine, Kobe 650-0017, Japan*
[b] *Kobe Pharmaceutical University, Kobe 658-8558, Japan*
[c] *Department of Pediatrics, Universiti Sains Malaysia, Kelantan 16150, Malaysia*
[d] *Department of Pediatrics, Osaka University Graduate School of Medicine, Osaka 565-0871, Japan*
[e] *Department of Pediatrics, Bell Land General Hospital, Sakai 599-8247, Japan*
[f] *Department of Pediatric Neurology, Morinomiya Hospital, Osaka 536-0023, Japan*
[g] *Institute of Medical Genetics, Tokyo Women's Medical University, Tokyo, Japan*
[h] *Department of Pediatrics, Kobe University Graduate School of Medicine, Kobe 650-0871, Japan*
[i] *Division of Child Neurology, Department of Neurology, National Hospital Organization Toneyama National Hospital, Toyonaka, Japan*

Received 4 August 2014; received in revised form 22 September 2014; accepted 6 October 2014

Abstract

Background: More than 90% of spinal muscular atrophy (SMA) patients show homozygous deletion of *SMN1* (survival motor neuron 1). They retain *SMN2*, a highly homologous gene to *SMN1*, which may partially compensate for deletion of *SMN1*. Although the promoter sequences of these two genes are almost identical, a GCC insertion polymorphism has been identified at c.-320_-321 in the *SMN1* promoter. We have also found this insertion polymorphism in an *SMN2* promoter in an SMA patient (Patient A) who has SMA type 2/3.

Purpose: The aims of this study were to determine the frequency of the GCC insertion polymorphism in SMA patients, and to evaluate its effect on *SMN* transcription efficiency.

Patients and methods: Fifty-one SMA patients, including Patient A, were involved in this study. *SMN2* transcript levels in white blood cells were measured by real-time polymerase chain reaction. Screening of the GCC insertion polymorphism was performed using denaturing high-pressure liquid chromatography. The transcription efficiency of the promoter with the insertion mutation was evaluated using a reporter-gene assay.

Results: All SMA patients in this study were homozygous for *SMN1* deletion. Patient A retained two copies of *SMN2*, and showed only a small amount of *SMN2* transcript in white blood cells. We detected a GCC insertion polymorphism at c.-320_-321 only in Patient A, and not in 50 other SMA patients. The polymorphism had a slight but significant negative effect on transcription efficiency.

Discussion and conclusion: Patient A was judged to be an exceptional case of SMA, because the GCC insertion polymorphism rarely exists in *SMN1*-deleted SMA patients. The GCC insertion polymorphism did not enhance the transcriptional efficiency of

* Corresponding author at: Department of Community Medicine and Social Healthcare Science, Kobe University Graduate School of Medicine, 7-5-1 Kusunoki-cho, Chuo-ku, Kobe 650-0017, Japan. Tel.: +81 78 382 5540; fax: +81 78 382 5559.
E-mail address: nishio@med.kobe-u.ac.jp (H. Nishio).

http://dx.doi.org/10.1016/j.braindev.2014.10.006

Please cite this article in press as: Harahap NIF et al. Trinucleotide insertion in the *SMN2* promoter may not be related to the clinical phenotype of SMA.. Brain Dev (2014), http://dx.doi.org/10.1016/j.braindev.2014.10.006

SMN2. Thus, this GCC insertion polymorphism in the *SMN2* promoter may not be associated with the milder phenotype of the patient. Patient A suggests that there are other unknown factors modifying the clinical phenotype of SMA.

Keywords: Spinal muscular atrophy; *SMN1*; *SMN2*; Promoter; Polymorphism

1. Introduction

Spinal muscular atrophy (SMA) is an autosomal recessive neuromuscular disorder characterized by proximal muscular atrophy of the limbs and trunk, resulting from degeneration of motor neurons in the anterior horn of the spinal cord. The incidence of the disease has been estimated at 1 in 6000–10,000 newborns, with an expected carrier frequency of 1 in 40–50 [1].

SMA is classified into three clinical subtypes depending on the age of disease onset and the achievement of motor milestones [2]: type 1 (severe form, Werdnig-Hoffmann disease; age of onset 0–6 months, unable to sit unaided), type 2 (Dubowitz disease, intermediate form; age of onset <18 months, unable to stand or walk unaided), and type 3 (mild form; Kugelberg–Welander disease; age of onset >18 months, able to stand or walk unaided). Additionally, two other forms of the disease, with the most severe having prenatal onset and the mildest type manifesting after 20 years of age, have been reported as SMA type 0 (prenatal form) and SMA type 4 (adult form) [3].

Using linkage analysis, all clinical subtypes of SMA have been mapped to chromosome 5q11.2–13.3. The survival motor neuron (*SMN*) gene has been identified as a candidate for SMA [4]. *SMN* is in fact two highly homologous genes, *SMN1* (the telomeric copy) and *SMN2* (the centromeric copy) [4]. *SMN1* and *SMN2* encode the same protein; however, *SMN1* is now considered to be responsible for the development of SMA, because its homozygous deletion has been found in >90% of SMA patients, and subtle but deleterious intragenic *SMN1* mutations have been identified in non-deletion patients [4,5]. It has been accepted that *SMN2* may be a modifier gene of SMA. Owing to a single nucleotide difference between *SMN1* and *SMN2*, exon 7 of *SMN2* is alternatively spliced (more precisely, skipped) resulting in the production of an *SMN* transcript lacking exon 7 (Δ7-*SMN* transcript) and an unstable Δ7-SMN protein [6]. The single nucleotide change in *SMN2* exon 7, which is a C-to-T transition located at codon 280, increases Δ7-*SMN* transcript levels and, correspondingly, decreases full-length *SMN* (FL-*SMN*) transcript levels [7]. Even so, *SMN2* is also able to generate a small amount of full-length transcript, and thus it can partially compensate the loss of *SMN1* [8].

Generally, the clinical severity of SMA patients is inversely correlated with *SMN2* copy number. A high copy number of *SMN2* is associated with a milder phenotype, and a low copy number with a more severe phenotype. SMA type 1 patients typically have two copies of *SMN2*, SMA type 2 patients have three copies, and SMA type 3 patients typically have three or more copies [9]. More than four *SMN2* copies are associated with a milder phenotype of SMA type 3 [10]. However, the clinical severity cannot always be determined by the *SMN2* copy number alone.

The expression level of *SMN2* may also be correlated with the clinical severity of the disease and, therefore, analysis of the *SMN2* promoter is important. Echaniz-Laguna et al. and Boda et al. reported that the promoter sequences of *SMN1* and *SMN2* are identical, providing strong evidence for similar transcriptional regulation of these genes [11,12]. However, Monani et al. found more than 10 nucleotide differences between the promoter regions of these two genes [13,14]. One of them, a GCC insertion polymorphism, was specifically identified at c.-320_-321 in the *SMN1* promoter, leading to GCC duplication at c.-324–c.-318. Polymorphisms in the promoter region may have some effect on transcriptional activity.

We found the GCC insertion polymorphism in an *SMN2* promoter in a Japanese boy diagnosed as having SMA type 2/3 (Patient A). The location of the GCC insertion in the *SMN2* promoter in Patient A was corresponding to that of the GCC in the *SMN1* promoter reported by Monani et al. [14]. It is notable that the clinical phenotype of the patient was much milder than expected based on his *SMN2* copy number. In this study, we determined the frequency of the GCC insertion polymorphism in controls and SMA patients. We also evaluated the effect of the GCC insertion polymorphism on *SMN2* transcriptional activity.

2. Patients and methods

2.1. Patients

All 50 Japanese patients in this study fulfilled the diagnostic criteria defined by the 59th ENMC International Workshop [2]; 26 patients (aged 1–34 years) were type 1, 16 type 2, and eight type 3. The molecular genetic analysis was approved by the Ethical Committee of the Kobe University Graduate School of Medicine, Japan. Informed consent was obtained from the patients or their parents. Fifty healthy Japanese adults (aged 21–

Please cite this article in press as: Harahap NIF et al. Trinucleotide insertion in the *SMN2* promoter may not be related to the clinical phenotype of SMA.. Brain Dev (2014), http://dx.doi.org/10.1016/j.braindev.2014.10.006

70 years) volunteered to participate in the study as control subjects.

Patient A was a 2-year-old Japanese boy who was clinically suspected as having a neuromuscular disorder with decreased muscle tonus. He was born as the third child to non-consanguineous and healthy parents. The pregnancy and delivery were non-eventful. Early developmental milestones were slightly delayed: head control was obtained at age 6 months, sitting without support at age 8 months, crawling at age 9 months, and standing and walking with support (ex. handrails) at age 18 months. However, he could never walk without support. He uttered his first word at 18 months, and a simple two-word sentence at 22 months. On admission, his weight and height were 85.5 cm (−0.7 SD) and 11.5 kg (−0.9 SD). His mental status was alert. Apparent facial anomaly was absent, but high-arched palate was present. Lung and heart auscultation revealed no abnormal findings. Abdominal examination was normal. Tongue fasciculation was absent. Muscle tonus was decreased: scarf sign, heel-to-ear sign, and loose-shoulder sign were observed. Muscle strength was also decreased especially in the proximal region of the legs. Deep tendon reflexes were absent or extremely diminished. Laboratory examination revealed no muscular damage (AST 28 IU/L, ALT 10 IU/L, CK 119 IU/L, ALD 7 IU/L, lactate 13 mg/dL, pyruvate 0.8 mg/dL). Muscle biopsy findings were compatible with those of SMA. Based on the muscle biopsy findings, together with the clinical phenotype, he was diagnosed as having SMA type 2/3.

2.2. *SMN1* deletion test and *SMN2* gene dosage analysis

Genomic DNA was extracted from peripheral white blood cells. The *SMN1* exon 7 deletion test was performed by the PCR-restriction fragment length polymorphism method of van der Steege et al. [15]. *SMN2* copy numbers were determined with a LightCycler 1.5 instrument (Roche Diagnostics GmbH, Mannheim, Germany) using FastStart DNA Master SYBR Green I (Roche Diagnostics) according to the method of Tran et al. [16].

2.3. RNA extraction, cDNA synthesis, and quantitative real-time PCR

Total RNA was isolated from peripheral white blood cells. cDNA was synthesized from total RNA with Transcriptor Reverse Transcriptase (Roche Diagnostics) according to the manufacturer's instructions.

Quantitative reverse-transcription-PCR was performed with a LightCycler 1.5 instrument (Roche Diagnostics) using FastStart DNA Master SYBR Green I (Roche Diagnostics). To evaluate transcript levels of the *SMN* genes, we amplified cDNA fragments of exons 1–2b, exons 7 and 8, and exons 5, 6 and 8. The cDNA fragment including exons 1–2b represented total *SMN* transcript, because the sequence of exons 1–2b is commonly included in all transcript isoforms. The cDNA fragment containing exons 7 and 8 represented the FL-*SMN* transcript, because it contained sequence beyond exon 7. The cDNA fragment including *SMN* exons 5, 6 and 8 represented the Δ7-*SMN* transcript, because it did not carry the sequence of exon 7. We used glyceraldehyde-3-phosphate dehydrogenase (*GAPDH*) as an endogenous reference gene, and the levels of *SMN* were normalized relative to those of *GAPDH*. The primers for the total-*SMN*, FL-*SMN*, Δ7-*SMN*, and *GAPDH* transcripts have been described previously [17,18]. Quantitation of the PCR products was performed with the second derivative maximum method of the LightCycler software.

2.4. Denaturing high-pressure liquid chromatography (DHPLC) detection of GCC insertion polymorphism in the SMN promoter

To screen for the GCC insertion polymorphism in SMA patients and controls, DHPLC analysis of PCR products was performed. PCR of the fragment including the polymorphism site was carried out with the primer set: 5′-tgcaatgagccgagatggtg-3′ and 5′-cctccccctttggaaaagtaa-3′. The PCR products were then directly loaded into the autosampler of an automated DHPLC system, the WAVE Nucleic Acid Fragment Analysis System, equipped with a DNASep cartridge (Transgenomic, Omaha, NE, USA). The samples were run under partially denaturing conditions at 54.6 °C (oven temperature). The buffer gradient conditions were the same as previously reported [19].

2.5. Sequencing

Direct and/or subcloned sequencing analyses of PCR-amplified products were performed. Sequencing reactions were performed using a dye terminator cycle-sequencing kit (Applied Biosystems/Life Technologies Corporation, Carlsbad, CA, USA), according to the supplier's instructions. The reaction products were automatically electrophoresed on an ABI PRISM 310 Sequencer (Applied Biosystems) and then analyzed using the Sequencing Software Module provided with the ABI PRISM 310 Sequencer.

2.6. Preparation of expression vectors

The PCR-amplified fragment containing GCCGCC polymorphism or GCC polymorphism was inserted into a firefly luciferase reporter plasmid, pGL2BTK (pGL2-Basic with a minimal herpes virus 1 thymidine kinase promoter). The GCCGCC and GCC fragment-containing plasmids were designated as 'pGCCGCC'

Please cite this article in press as: Harahap NIF et al. Trinucleotide insertion in the *SMN2* promoter may not be related to the clinical phenotype of SMA.. Brain Dev (2014), http://dx.doi.org/10.1016/j.braindev.2014.10.006

and 'pGCC', respectively. The construct maps of pGL2BTK, pGCCGCC, and pGCC are shown in Fig. 1.

2.7. Transcription assay

The responses of the test plasmids (pGL2BTK, pGCCGCC, pGCC) to dibutyryl cAMP (dbcAMP; 0.5 mM), forskolin (20 μM), and a combination of dibutyryl cAMP and forskolin were determined in a human neuroblastoma cell line, BE(2)-C cells. The neuroblastoma cell lines have been used as useful experimental models of neuronal differentiation because the morphological, biochemical and electrophysiological properties of neuroblastoma cell lines are similar to those of neurons [20].

Neuroblastoma cells [2×10^5 cells in Minimum Essential Medium (MEM)] were cotransfected with a test plasmid (1.6 μg) and the phRL plasmid (a sea pansy luciferase reporter plasmid; Promega Corporation, Madison, WI, USA) (0.5 ng) using Lipofectamine 2000 (Invitrogen/Life Technologies Corporation). Twenty-four hours after transfection, dibutyryl cAMP, forskolin, or a combination of dibutyryl cAMP and forskolin was added to the MEM. The cells were harvested after culture for an additional 24 h.

Transcriptional activity of the test plasmids was measured using the dual-luciferase reporter assay system, in which sea pansy-luciferase activity was used as a control for the transfection efficiency of the test plasmids. Each transcriptional activity measurement was repeated three times and the data are expressed as the mean ± SD.

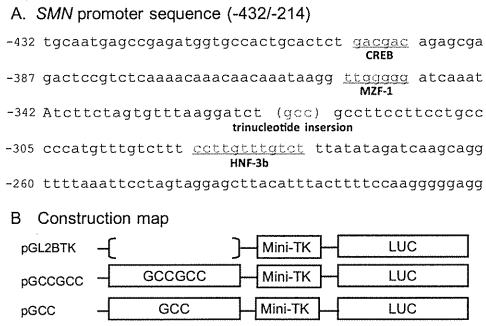

Fig. 1. *SMN* promoter sequence (A) and construction map (B). The *SMN* promoter sequence from c.-432 to c.-214 is shown in the upper part of the figure (A). The numbering of nucleotide in the promoter sequence is based on Monani et al. [14]. Trinucleotide insertion at c.-320_-321 is parenthesized. Putative transcription factor binding sites are underlined. Plasmid construction map is shown in the lower part of the figure (B). All constructs have a firefly-luciferase reporter gene, which is designated as LUC in the map. The pGL2BTK plasmid is a basic plasmid served as control. The GCCGCC and GCC fragment-containing plasmids were designated as 'pGCCGCC' and 'pGCC', respectively.

2.8. Statistics

Statistical analysis of the transcriptional activity data was performed using Microsoft Excel 2003 software and Statistical Package for the Social Sciences (SPSS Inc., Chicago, I, USA). The Student's *t*-test was conducted to evaluate differences between the plasmids. A probability of less than 0.05 was considered statistically significant.

3. Results

3.1. SMN1 deletion test and SMN2 gene dosage analysis

We performed an *SMN1* deletion test on Patient A, who was suspected as having SMA type 2/3. The patient carried zero copies of *SMN1* and two copies of *SMN2*. Based on molecular analysis, he was diagnosed as having SMA.

A nucleotide substitution in *SMN2* exon 7, c.859G>C, has been reported as a positive modifier of the SMA phenotype [21,22]. To check whether the mutation is present in Patient A, we performed a sequencing analysis of the exon 7. However, we did not find any substitutions including c.859G>C.

3.2. SMN2 transcript levels

Our aim of this study was to compare the *SMN2* transcript levels of Patient A to those of other SMA type 2 patients, because we hypothesized that *SMN2* transcript expression was the key determinant of the SMA phenotype. It would have been preferable to compare Patient A with SMA type 2 patients carrying two copies of *SMN2*. However, we did not have cDNA samples from SMA type 2 patients with zero copies of *SMN1* and two copies of *SMN2*. In this study, we determined the baseline transcript levels of total *SMN*, FL-*SMN*, and Δ7-*SMN* in the white blood cells of Patient A, five disease controls (DCs 1–5; they were all SMA type 2 patients with zero copies of *SMN1* and three copies of *SMN2*) and three healthy controls. All of the disease controls were able to sit without support, but could not stand or walk even with any support.

Total *SMN* transcript levels of Patient A, DC1, DC2, DC3, DC4, and DC5 were 38%, 76%, 66%, 181%, 232%, and 166% of the mean value of the healthy controls, respectively. This finding suggested that *SMN2* transcription in Patient A was significantly reduced compared with that of the disease controls.

The FL-*SMN* transcript levels of Patient A, DC1, DC2, DC3, DC4, and DC5 were 53%, 58%, 64%, 44%, 68%, and 95% of the mean value of the healthy controls, respectively. The Δ7-*SMN* transcript levels of Patient A, DC1, DC2, DC3, DC4, and DC5 were 167%, 206%, 130%, 130%, 97%, and 145% of the mean value of the healthy controls, respectively. These findings suggested

Please cite this article in press as: Harahap NIF et al. Trinucleotide insertion in the *SMN2* promoter may not be related to the clinical phenotype of SMA.. Brain Dev (2014), http://dx.doi.org/10.1016/j.braindev.2014.10.006

that *SMN2* splicing in Patient A was similar to that of the disease controls.

3.3. Identification of GCC polymorphism in the SMN2 promoter

According to Monani et al., a ~200-bp element lying between −441 and −228 (numbering is based on the article of Monani et al. [14]) in *SMN* promoters drives strong expression. Thus, we explored the *SMN2* promoter of Patient A. Direct sequence analysis of the element showed overlapping nucleotide peaks (Fig. 2), suggesting an insertion or deletion of some nucleotides. Sequencing analysis of subcloned fragments identified two different alleles with and without a GCC insertion at position c.-320_-321. However, no other mutations were detected in this region.

The Ag1CA multicopy microsatellite marker sequence is present in the promoter region downstream of the GCC insertion at c.-320_-321. Therefore, the GCC location may be different from allele to allele. We did not identify the real size of the Ag1CA multicopy marker sequence or the real position of the GCC insertion in Patient A. The GCC insertion at c.-320_-321 does not represent the real location in Patient A. In this study, based on the report by Monani et al. [14], we named this GCC insertion polymorphism in the *SMN1/SMN2* promoter as "the GCC insertion at c.-320_-321").

3.4. Frequency of GCC insertion in control individuals and SMA patients

We performed DHPLC screening for the GCC insertion polymorphism in 50 control individuals and 50 SMA patients (Patient A was not included in the 50 SMA patients) (Fig. 3). All control individuals carried *SMN1* and *SMN2*, and all SMA patients lacked *SMN1* but retained *SMN2*.

The GCC insertion polymorphism was found in 12 out of 50 control individuals (24%), while it was not found in any SMA patients. Using long-range PCR, we also confirmed that the GCC insertion polymorphism was present in the *SMN1* promoter in a healthy control. However, the GCC insertion polymorphism was absent in all SMA patients (Table 1). This observation suggested that the GCC insertion polymorphism propagates mainly in *SMN1* genes.

3.5. Effects of GCC insertion on transcription efficiency in luciferase transcription assay

To clarify the effect of the GCC insertion polymorphism on transcription activity, we performed transient transfection experiments with pGL2BTK, pGCCGCC, and pGCC (Fig. 4). The sequences of inserted fragments, GCCGCC and GCC, are presented in Fig. 1. It should be noted that the cyclic AMP-response element (CRE)-like site, TGACGACA, is present at 84 bp upstream of the polymorphism position.

Neuroblastoma cell lines have been used because of their closely resembled characteristic of neurons. In the assay with neuroblastoma cell lines, BE(2)-C cells, the baseline activity of pGCCGCC was lower than that of pGCC. Furthermore, the response to dibutyryl cAMP (a cyclic nucleotide derivative which mimics the action of endogenous cAMP), forskolin (a reagent elevating cAMP via activation of the adenylyl cyclase), or both reagents was slightly lower in pGCCGCC than in pGCC. These results suggested that the presence of the GCC insertion polymorphism slightly decreased transcription efficiency of the *SMN2* promoter in neuronal cells. Thus, the GCC insertion polymorphism in the *SMN2* promoter of Patient A may not increase, but decrease transcription efficiency. This finding was

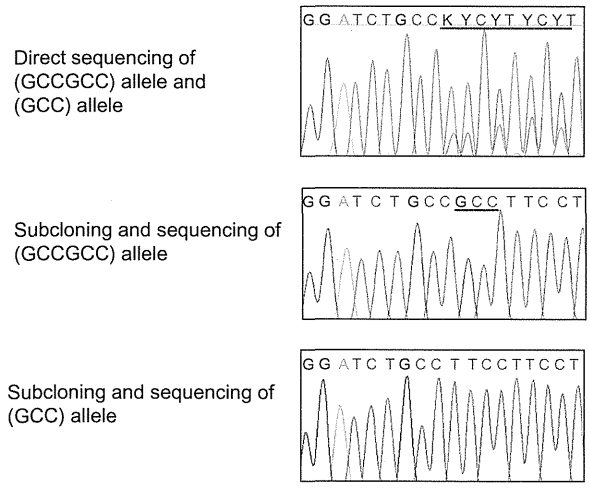

Fig. 2. Sequencing of the *SMN2* promoter region of Patient A. Direct sequencing analysis showed overlapping nucleotide peaks suggesting the presence of two different alleles (top). Subcloning sequencing analysis separately identified (GCCGCC) allele and (GCC) allele (middle and bottom).

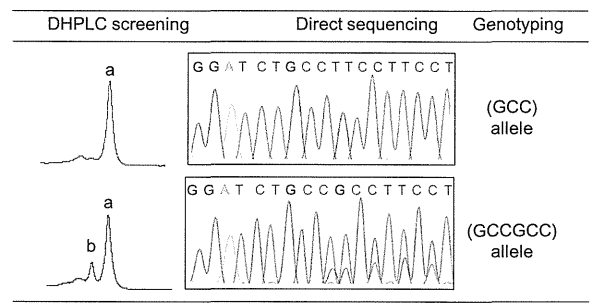

Fig. 3. DHPLC screening for the GCC insertion polymorphism. DHPLC analysis for the (GCC) allele showed a single peak (a-peak), but the presence of (GCCGCC) allele generated an additional peak (b-peak) to the a-peak.

Please cite this article in press as: Harahap NIF et al. Trinucleotide insertion in the *SMN2* promoter may not be related to the clinical phenotype of SMA.. Brain Dev (2014), http://dx.doi.org/10.1016/j.braindev.2014.10.006

Table 1
Frequency of GCC insertion polymorphism in control individuals and *SMN1*-deleted SMA patients.

	GCC insertion polymorphism		
	Present	Absent	
SMN1-deleted SMA patients*	0	50	50
Healthy control individuals	12	38	50
	12	88	100

* Patient A was excluded from the *SMN1*-deleted SMA patients.

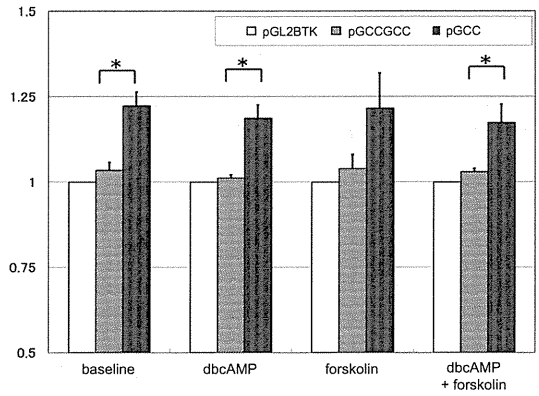

Fig. 4. Effect of GCC insertion polymorphisms on transcriptional activity. The effect of the GCC insertion polymorphism on transcription activity after transient transfection with pGL2BTK, pGCCGCC and pGCC into a neuroblastoma cell line, BE(2)-C cells. According to our data, the presence of the GCC insertion polymorphism slightly decreased transcription efficiency of the *SMN2* promoter in neuronal cells, with or without dibutyryl cAMP (dbcAMP) and/or forskolin treatment. The asterisk (*) shows the significant difference ($p < 0.01$).

compatible with a decreased amount of total *SMN2* transcript in white blood cells of Patient A.

4. Discussion

4.1. SMN2 copy number analysis

In this study, we presented a *SMN1*-deleted SMA patient with two copies of *SMN2*. He showed a milder phenotype than we had expected based on a low *SMN2* copy number. Patient A was able to sit without support, and also able to take a few steps sideways when supported. The clinical phenotype of the patient was judged to be SMA type 2/3, or type 2.9 according to the classification of Dubowitz [23].

Feldkötter et al. [24] reported that 138 out of 153 patients carrying two copies of *SMN2* were type 1 patients (90%). Swoboda et al. [25] reported that 21 out of 22 patients carrying two copies of *SMN2* were ventilator dependent or unable to sit unsupported (95%). These results are fully compatible with our previous observation of 37 out of 39 patients carrying two copies of *SMN2* being diagnosed as SMA type 1 [26].

Even though the *SMN2* copy number is a modifying factor of the SMA phenotype, there are some exceptional cases. Prior et al. and Vezain et al. reported that some unrelated SMA patients with 1–2 copies showed much milder clinical phenotypes than expected [20,21]. They identified a single base substitution, c.859G>C, in *SMN2* exon 7, leading to inclusion of the exon in *SMN2* mRNA. Patient A may also belong to such a patient group with a discrepancy between clinical phenotype and *SMN2* copy number. However, Patient A did not carry a c.859G > C substitution.

Recently, Oprea et al. reported the possibility of a female-specific modifying factor [27]. They suggested that high plastin 3 (*PLS3*) expression may be a female-specific modifying factor, which was observed in non-symptomatic females lacking *SMN1* (discussed further below). However, Patient A was a male, not a female.

It is, therefore, reasonable to think that unknown modifiers, other than an increase of *SMN2* copy number, the presence of an *SMN2* mutation facilitating exon 7 inclusion or a female-specific modifying factor, ameliorated the phenotype of this patient.

We found a GCC insertion polymorphism at c.-320_-321 in the *SMN2* promoter of Patient A. This trinucleotide insertion has already been identified in *SMN1*, but not in *SMN2*. Monani et al. [13] found more than 10 nucleotide differences between the *SMN* promoter regions of PAC 125D9 and PAC 125D15. Among them, a GCC insertion polymorphism was found in PAC 125D9 containing *SMN1*, but not in PAC 125D15 containing *SMN2* [13]. However, Boda et al. reported that the promoter sequences of *SMN1* and *SMN2* were identical [12]. They suggested that the different nucleotides in the sequence of PAC 125D9, including the GCC insertion, could be accounted for by errors in the sequencing of this clone.

Our study demonstrates that the GCC insertion polymorphism is, without doubt, present in the human population. The GCC insertion polymorphism was found in one fourth of control individuals, but was absent in all SMA patients, except for Patient A. In addition, strictly speaking, the possibility exists that in Patient A the upstream region, including the *SMN1* promoter, was connected to the downstream region, including *SMN2* exons, during gene conversion switching. These findings suggest that the GCC insertion polymorphism is perpetuated in *SMN1* genes.

4.2. Effect of the GCC insertion polymorphism on transcriptional activity

Next, we examined the possibility of the GCC insertion polymorphism in *SMN2* as a modifying factor of the SMA phenotype. Comparison between patient A (two copies of *SMN2*) and other SMA type 2 patients

Please cite this article in press as: Harahap NIF et al. Trinucleotide insertion in the *SMN2* promoter may not be related to the clinical phenotype of SMA.. Brain Dev (2014), http://dx.doi.org/10.1016/j.braindev.2014.10.006

(three copies of *SMN2*) revealed a lower total *SMN* transcript level in peripheral blood cells of patient A. This finding suggests that the *SMN2* transcript level in patient A is mainly influenced by *SMN2* gene dosage. However, we are unable to examine *SMN2* transcription in motor neurons.

Monani et al. [14] showed that a ~200-bp fragment lying between −441 and −228 (numbering is based on the article of Monani et al. [14]) drives strong expression in a motor neuron cell line. The ~200-bp fragment contains a CRE-like site (TGACGACA), which interacts with the cyclic-AMP responsive element binding protein (CREB). Because the GCC insertion polymorphism resides in this fragment, we suggest that it may exert a negative (suppressing) or positive (enhancing) effect on transcriptional efficiency.

To examine the effect of the polymorphism on transcriptional efficiency, we constructed plasmids containing the ~200-bp fragment, and performed a luciferase reporter gene analysis using a neuroblastoma cell line (as an alternative cell line of a motor neuron cell line). Under baseline conditions and stimulated conditions with dbcAMP, forskolin, or both reagents, luciferase activity of the plasmid construct with the GCC insertion was lower compared with that without the GCC insertion.

These data suggest that the presence of the GCC insertion polymorphism slightly decreases transcription efficiency of the *SMN2* promoter in neuronal cells. Thus, the GCC insertion polymorphism in the *SMN2* promoter of Patient A might partially decrease transcription efficiency.

However, we must mention some limitations of this study. First, we do not know whether the *SMN2* promoter of Patient A carries any polymorphisms other than the GCC insertion polymorphism. The existence or not of other polymorphisms should be determined for a more accurate evaluation of the promoter function. Furthermore, the promoter region that we used to study *SMN2* transcription efficiency was not large enough to evaluate the combined effect of promoter-binding proteins, although the *SMN2* transcript levels of Patient A were significantly lower than those of other individuals tested in this study.

4.3. Modifying genes outside SMN genes

Our data show that FL-*SMN* transcript levels in Patient A were similar to those in five other SMA patients with three copies of *SMN2*. The amount of FL-*SMN* transcript is regulated by two processes, transcriptional activity and splicing of exon 7; however, transcription was not up-regulated in this patient. Patient A, therefore, suggests positive effects of splicing-related factors on the increase in FL-*SMN* transcript levels and that the modifier gene in Patient A may be related to the splicing machinery. However, the phenotype of our patient was much milder compared with the phenotypes of patients with typical SMA type 2. This indicates that the phenotype was positively modified by factors other than FL-*SMN* transcript levels (and levels of FL-*SMN* protein).

It is certain that modifying factors other than *SMN* genes are closely related to the SMA phenotype. Recently, Oprea et al. reported the possibility of a female-specific modifying factor [27]. They suggested that high plastin 3 (*PLS3*) expression, observed in non-symptomatic females lacking *SMN1*, may be such a factor (discussed further below). However, Patient A was a male, not a female.

The presence of asymptomatic females with no *SMN1* copies strongly suggests that non-*SMN* genes may be related to the pathogenesis or anti-pathogenesis of SMA. In this context, it is also necessary to clarify modifying factors other than *SMN* genes to establish an effective treatment for SMA.

4.4. Conclusion

In this study, we found a GCC insertion polymorphism at c.-320_-321 in the *SMN2* promoter of Patient A, an *SMN1*-deleted SMA patient with a milder phenotype than expected considering the low *SMN2* copy number. Transcription assays demonstrated that the polymorphism had a negative effect on transcription efficiency. This finding was compatible with a decreased amount of total *SMN2* transcript in white blood cells from Patient A. Thus, this GCC insertion polymorphism in the *SMN2* promoter may not be associated with the mild phenotype of the patient. Furthermore, our experiment in this study show that *SMN* gene and milder clinical phenotype of SMA may not always been correlated. We suggest non *SMN* gene factor maybe worked in this patient. Future studies are necessary to identify the modifying genes outside *SMN* gene that ameliorated the clinical phenotype of the patient.

Acknowledgments

This work was supported by a Grant-in-Aid from the Ministry of Education, Science, Sports and Culture of Japan (project number 22591127) and a Grant-in-Aid from the Research Committee of Spinal Muscular Atrophy (SMA), the Ministry of Health, Labour and Welfare of Japan.

References

[1] Nurputra DK, Lai PS, Harahap NIF, Morikawa S, Yamamoto T, Nishimura N, et al. Spinal muscular atrophy: from gene discovery to clinical trials. Ann Hum Genet 2013;77:435–63.

Please cite this article in press as: Harahap NIF et al. Trinucleotide insertion in the *SMN2* promoter may not be related to the clinical phenotype of SMA.. Brain Dev (2014), http://dx.doi.org/10.1016/j.braindev.2014.10.006

[2] Zerres K, Davies KE. 59th ENMC international workshop: spinal muscular atrophies: recent progress and revised diagnostic criteria. Neuromusc Disord 1999;9:272–8.
[3] Kolb SJ, Kissel JT. Spinal muscular atrophy: a timely review. Arch Neurol 2011;68:979–84.
[4] Lefebvre S, Bürglen L, Reboullet S, Clermont O, Burlet P, Viollet L, et al. Identification and characterization of a spinal muscular atrophy-determining gene. Cell 1995;80:155–65.
[5] Sun Y, Grimmler M, Schwarzer V, Schoenen F, Fischer U, Wirth B. Molecular and functional analysis of intragenic SMN1 mutations in patients with spinal muscular atrophy. Hum Mutat 2005;25:64–71.
[6] Lorson CL, Strasswimmer J, Yao JM, Baleja JD, Hahnen E, Wirth B, et al. *SMN* oligomerization defect correlates with spinal muscular atrophy severity. Nat Genet 1998;19:63–6.
[7] Lorson CL, Hahnen E, Androphy EJ, Wirth B. A single nucleotide in the *SMN* gene regulates splicing and is responsible for spinal muscular atrophy. Proc Natl Acad Sci USA 1999;96:6307–11.
[8] Lefebvre S, Burlet P, Liu Q, Bertrandy S, Clermont O, Munnich A, et al. Correlation between severity and SMN protein level in spinal muscular atrophy. Nat Genet 1997;16:265–9.
[9] Harada Y, Sutomo R, Sadewa AH, Akutsu T, Takeshima Y, Wada H, et al. Correlation between *SMN2* copy number and clinical phenotype of spinal muscular atrophy: three *SMN2* copies fail to rescue some patients from the disease severity. J Neurol 2002;249:1211–9.
[10] Wirth B, Brichta L, Hahnen E. Spinal muscular atrophy: from gene to therapy. Semin Pediatr Neurol 2006;13:121–31.
[11] Echaniz-Laguna A, Miniou P, Bartholdi D, Melki J. The Promoters of the survival motor neuron gene (*SMN*) and its copy (*SMNc*) share common regulatory elements. Am J Hum Genet 1999;64:1365–70.
[12] Boda B, Mas C, Giudicelli C, Nepote V, Guimiot F, Levacher B, et al. Survival motor neuron *SMN1* and *SMN2* gene promoters: identical sequences and differential expression in neurons and non-neuronal cells. Eur J Hum Genet 2004;12:729–37.
[13] Monani UR, Lorson CL, Parsons DW, Prior TW, Androphy EJ, Burghes AHM, et al. A single nucleotide difference that alters splicing patterns distinguishes the SMA gene *SMN1* from the copy gene *SMN2*. Hum Mol Genet 1999;8:1177–83.
[14] Monani UR, McPherson JD, Burghes AHM. Promoter analysis of the human centromeric and telomeric survival motor neuron genes (SMN^C and SMN^T). Biochim Biophys Acta 1999;1445:330–6.
[15] van der Steege G, Grootscholten PM, van der Vlies P, Draaijers TJ, Osinga J, Cobben JM, et al. PCR-based DNA test to confirm clinical diagnosis of autosomal recessive spinal muscular atrophy. Lancet 1995;345:985–6.
[16] Tran VK, Sasongko TH, Hong DD, Hoan NT, Dung VC, Lee MJ, et al. *SMN2* and *NAIP* gene dosages in Vietnamese patients with spinal muscular atrophy. Pediatr Int 2008;50:346–51.
[17] Riessland M, Brichta L, Hahnen E, Wirth B. The benzamide M344, a novel histone deacetylase inhibitor, significantly increases SMN2 RNA/protein levels in spinal muscular atrophy cells. Hum Genet 2006;120:101–10.
[18] Harahap ISK, Saito T, San LP, Sasaki N, Gunadi Nurputra DKP, et al. Valproic acid increases SMN2 expression and modulates SF2/ASF and hnRNPA1 expression in SMA fibroblast cell lines. Brain Dev 2012;34:213–22.
[19] Sutomo R, Akutsu T, Takeshima Y, Nishio H, Sadewa AH, Harada Y, et al. Rapid *SMN1* deletion test using DHPLC to screen patients with spinal muscular atrophy. Am J Med Genet 2002;113:225–6.
[20] Wu G, Fang Y, Lu ZH, Ledeen RW. Induction of axon-like and dendrite-like processes in neuroblastoma cells. J Neurocytol 1998;27:1–14.
[21] Prior TW, Krainer AR, Hua Y, Swoboda KJ, Snyder PC, Bridgeman SJ, et al. A positive modifier of spinal muscular atrophy in the *SMN2* gene. Am J Hum Genet 2009;85:408–13.
[22] Vezain M, Saugier-Veber P, Goina E, Touraine R, Manel V, Toutain A, et al. A rare *SMN2* variant in a previously unrecognized composite splicing regulatory element induces exon 7 inclusion and reduces the clinical severity of spinal muscular atrophy. Hum Mutat 2010;31:E1110–25.
[23] Dubowitz V. Chaos in the classification of SMA: a possible resolution. Neuromuscul Disord 1995;5:3–5.
[24] Feldkötter M, Schwarzer V, Wirth R, Wienker TF, Wirth B. Quantitative analyses of SMN1 and SMN2 based on real-time lightcycler PCR: fast and highly reliable carrier testing and prediction of severity of spinal muscular atrophy. Am J Hum Genet 2002;70:358–68.
[25] Swoboda KJ, Prior TW, Scott CB, McNaught TP, Wride MC, Reyna SP, et al. Natural history of denervation in SMA: relation to age, *SMN2* copy number, and function. Ann Neurol 2005;57:704–12.
[26] **Yamamoto T, Sato H, Lai PS, Nurputra DK, Harahap NIF, Morikawa S, et al. Intragenic mutations in *SMN1* may contribute more significantly to clinical severity than *SMN2* copy numbers in some spinal muscular atrophy (SMA) patients. Brain Dev 2013 (in press). doi: 10.1016/j.braindev.2013.11.009.**
[27] Oprea GE, Kröber S, McWhorter ML, Rossoll W, Müller S, Krawczak M, et al. Plastin 3 is a protective modifier of autosomal recessive spinal muscular atrophy. Science 2008;320:524–7.

Please cite this article in press as: Harahap NIF et al. Trinucleotide insertion in the *SMN2* promoter may not be related to the clinical phenotype of SMA.. Brain Dev (2014), http://dx.doi.org/10.1016/j.braindev.2014.10.006

doi:10.1111/ncn3.140

ORIGINAL ARTICLE

A Study of valproic acid for patients with spinal muscular atrophy

Toshio Saito,[1] Dian K Nurputra,[2,3] Nur Imma F Harahap,[2,3] Indra Sari K Harahap,[2,3] Hiroshi Yamamoto,[4] Emi Muneshige,[4] Hiroaki Nishizono,[4] Tsuyoshi Matsumura,[5] Harutoshi Fujimura,[5] Saburo Sakoda,[5] Kayoko Saito[6] and Hisahide Nishio[2]

[1]Division of Child Neurology, Department of Neurology, Toneyama National Hospital, Toyonaka, Osaka, [2]Department of Community Medicine and Social Healthcare Science, Kobe University Graduate School of Medicine, Kobe, Japan, [3]Department of Neurology, Faculty of Medicine, Gadjah Mada University, Yogyakarta, Indonesia, [4] Departments of Rehabilitation, [5] Neurology, Toneyama National Hospital, Toyonaka, Osaka, and [6]Institute of Medical Genetics, Tokyo Women's Medical University, Tokyo, Japan

Key words
Modified Hammersmith Functional Motor Scale for SMA, respiratory function, *SMN*, spinal muscular atrophy, valproic acid.

Accepted for publication 4 October 2014.

Correspondence
Toshio Saito
Division of Child Neurology, Department of Neurology, National Hospital Organization Toneyama National Hospital, 5-1-1 Toneyama, Toyonaka, Osaka, 560-8552 Japan. Email: saitot@toneyama.go.jp

Abstract

Background: Valproic acid (VPA) is expected to become an effective therapeutic agent for spinal muscular atrophy (SMA) because of its histone deacetylase inhibitor effect.

Aim: To evaluate the effectiveness of VPA for SMA.

Methods: Seven consecutive Japanese SMA patients (three males, four females) were recruited. Of those, six were type 2 (cases A–E, G) and one was type 3 (case F). One female patient (case E) was aged 2 years and 10 months, whereas the others ranged in age from 15 to 42 years. VPA was administered for 6 months with L-carnitine. We carried out *SMN* transcript analysis of peripheral white blood cells, and evaluated using the Modified Hammersmith Functional Motor Scale for SMA (MHFMS), vital capacity (VC), maximum insufflation capacity (MIC), and cough peak flow (CPF) before and at 1, 3 and 6 months after starting treatment.

Results: Cases B–E and G completed the study. The final VPA dosage in cases B–D and G was 400 mg/day, whereas that in case E was 100 mg/day. The quantity of the FL-*SMN* transcription product showed a tendency to increase. Case E showed a remarkable improvement in MHFMS, and gained motor function to turn from side to side during the study period. Although no significant changes were observed in MHFMS in the older cases, VC, MIC and CPF were improved in those.

Conclusion: Our findings suggest that VPA treatment is effective for improving MHFMS and respiratory function in some SMA patients. A placebo-controlled randomized trial is warranted to confirm the efficacy of VPA for SMA.

Introduction

Spinal muscular atrophy (SMA) is an autosomal recessive neuromuscular disorder characterized by degeneration of the anterior horn cells of the spinal cord, resulting in progressive muscular atrophy, and weakness of the limbs and trunk, with the incidence reported to be approximately one in 6000–10 000 live births.[1] SMA is classified into five groups; type 1 (Werdnig–Hoffman disease; severe form), type 2 (Dubowitz disease; intermediate form), type 3 (Kugelberg–Welander disease; mild form), type 4 (adult form) and type 0 (prenatal).[1–3]

The gene responsible for SMA is the survival motor neuron *(SMN)*, which exists as two highly homologous copies within the SMA gene region on chromosome 5q11.2–13.3, namely *SMN1* and *SMN2*.[4] The disease is caused by loss of *SMN1*, with more than 95% of SMA patients showing a homozygous deletion or interruption in *SMN1*, resulting in a deficiency of the SMN protein.[4–6] *SMN1* and *SMN2* are nearly identical, with the only difference being a single nucleotide change in the coding region, which shows that nucleotide +6 of exon 7 in *SMN1* is C and that of *SMN2* is T.

Although *SMN1* and *SMN2* encode the same protein because of a synonymous nucleotide change, *SMN2* does not fully compensate for the loss or dysfunction of *SMN1*. As the C to T change in *SMN2* at nucleotide position +6 in exon 7 induces exon skipping, *SMN1* and *SMN2* show different splicing patterns.[7,8] All *SMN1*-derived transcripts contain exon 7 and produce full-length *SMN* (FL-*SMN*),

whereas the majority of *SMN2*-derived transcripts lack exon 7 (Δ7-*SMN*).

Phenotypic variations in SMA are inversely correlated with *SMN2* copy number, and a higher *SMN2* copy number ameliorates the clinical phenotype.[1,9,10] *SMN2* might compensate for the loss of *SMN1* by modifying disease severity through production of a small amount of full-length SMN protein. Thus, treatment strategies for SMA have focused on increased production of the SMN protein from *SMN2*.

Valproic acid (VPA) is a histone deacetylase (HDAC) inhibitor as well as an anticonvulsant used for treatment of epileptic patients, as it increases SMN levels in SMA patients through activation of *SMN2* transcription and splicing correction of *SMN2* exon 7.[11,12] Its effects as a therapeutic agent of SMA are expected.[13–20] In the present study, we evaluated the efficacy of VPA in SMA patients.

Methods

The present study was carried out from January 2012 to March 2013.Seven consecutive Japanese SMA patients were recruited, of whom six were type 2 and one was type 3. The type 2 patients were as follows: case A, 34-year-old man; case B, 33-year-old woman; case C, 23-year-old man; case D, 30-year-old woman; case E, 2 years and 10-month-old girl; and case G, 15-year-old girl, whereas the type 3 patient was a 42-year-old man denoted as case F.

None of the participants possessed the *SMN1* gene, and had three copies of *SMN2* and the neuronal apoptosis inhibitory protein. All except for cases B and E used non-invasive ventilation at night. The demographic features of the patients are summarized in Table 1. All patients underwent physiotherapy, such as range of motion exercises of the extremities and respiration, before, during and after the study. The frequency and contents of physiotherapy differed among the patients, and were dependent on their situation including hospitalization, outpatient status and other factors.

VPA was given daily for 6 months to reach trough levels of 50–100 mg/dL, a dosing level typical of that used in epilepsy patients. L-carnitine was also given. We evaluated using the Modified Hammersmith Functional Motor Scale for SMA (MHFMS),[21] and also examined respiratory function and carried out *SMN* transcript analysis using quantitative real-time polymerase chain reaction (qRT–PCR) measurements with peripheral white blood cell samples[22] obtained from the patients before and 1, 3 and 6 months after starting VPA treatment. Blood samples were obtained from all patients in the daytime after fasting.

For *SMN* transcript analysis, we measured total-*SMN*, FL-*SMN* and Δ7-*SMN* transcript levels using qRT–PCR, with the latter two quantitated from the levels of the products encompassing *SMN* exons 7 and 8, and exons 5, 6 and 8, respectively. We used glyceraldehyde-3-phosphate dehydrogenase (*GAPDH*) as an endogenous reference gene, and the levels of *SMN* are expressed relative to those of *GAPDH*.[22] The detailed methods utilized for qRT–PCR have been described.[22] We also evaluated the ratio of FL-*SMN* to Δ7-*SMN* transcript (FL/Δ7-*SMN*). For respiratory function, we assessed vital capacity (VC), maximum insufflation capacity (MIC) and cough peak flow (CPF).[23,24] In addition, we also checked subjective symptoms, side-effects and bodyweight changes in each patient.

Statistical analysis. ANOVA with Tukey's or a Games–Howell *post-hoc* test were used to evaluate the differences in *SMN* transcript levels for each evaluation time. Statistical significance was accepted at $P < 0.05$.

Ethics. Written informed consent (for adults), or parental consent and assent (for children) were obtained for all participants. The study protocol was approved by the local ethical committees of Toneyama National Hospital and the University of Kobe.

Results

VPA and L-carnitine administration. Table 2 shows the dose of VPA administered and VPA concentration in each patient. Case A was eliminated before the 1-month evaluation because of sleepiness induced by VPA and discomfort caused by L-carnitine. Cases B–E and G completed

Table 1 Demographic features of patients with spinal muscular atrophy

Case	Sex	Age (years)	Type	*SMN1* exon7	*SMN1* exon8	*SMN2* copy number	NAIP	Respiratory status	Scoliosis	Motor function
A	Male	34	2	Delete	Delete	3	(+)	Night NPPV	(+++)	Assisted sitting
B	Female	33	2	Delete	Delete	3	(+)	Voluntary	(+)	Assisted sitting
C	Male	23	2	Delete	Delete	3	(+)	Night NPPV	(+++)	Assisted sitting
D	Female	30	2	Delete	Delete	3	(+)	Night NPPV + O2 inhalation in daytime	(+++)	Assisted sitting
E	Female	2 years 10 months	2	Delete	Delete	3	(+)	Voluntary	(+)	Assisted sitting
F	Male	42	3	Delete	Delete	3	(+)	Night NPPV	(+/-)	Sitting
G	Female	15	2	Delete	Delete	3	(+)	Night NPPV	(+)Spinal surgery	Assisted sitting

NAIP, neuronal apoptosis inhibitory protein; NPPV, non-invasive positive pressure ventilation.

Table 2 Results obtained from each patient. Dose of valproic acid, valproic acid concentration, score for Modified Hammersmith Functional Motor Scale for SMA, respiratory function, transcription amount of *SMN* and change in body weight.

Case	Time period (months)	VPA administration (mg)	VPA concentration (μg/mL)	MHFMS	VC (mL)	MIC (mL)	CPF (L/min)	FL-*SMN*	Δ7-*SMN*	FL/Δ7-*SMN*	Total -*SMN*	Body weight (kg)
A	Pre			0	965	–	115	0.51 (±0.06)	1.77 (±0.13)	0.28 (±0.02)	1.19 (±0.37)	
B	Pre			4	840	960	140	0.56 (±0.02)	1.12 (±0.19)	0.50 (±0.07)*	1.02 (±0.03)	31.4
	1	400	50	4	1000	810	95	0.80 (±0.05)	0.68 (±0.03)	1.17 (±0.03)*	5.47 (±2.11)	
	3	400	45	5	850	1000	165	0.86 (±0.35)	0.92 (±0.39)	0.95 (±0.14)	3.27 (±1.33)	
	6	400	42	5	810	1060	130	1.08 (±0.13)	0.58 (±0.26)	2.05 (±0.57)	1.61 (±0.13)	33.4
C	Pre			0	380	630	85	0.39 (±0.03)	2.02 (±0.47)	0.20 (±0.04)	2.82 (±0.67)	16
	1	200	39	0	400	600	90	0.49 (±0.09)	1.37 (±0.24)	0.36 (±0.07)	4.78 (±0.09)*,**	
	3	400	62	0	430	580	95	0.51 (±0.17)	1.16 (±0.76)	0.78 (±0.80)	2.96 (±0.34)*	
	6	400	75	0	500	710	100	0.45 (±0.24)	1.26 (±0.25)	0.39 (±0.27)	3.09 (±0.15)**	17.5
D	Pre			0	380	440	75	0.60 (±0.40)	0.83 (±0.13)	0.73 (±0.14)	3.61 (±0.19)*,**	19
	1	200	35	0	350	550	80	0.67 (±0.24)	1.13 (±0.13)	0.60 (±0.24)	2.96 (±1.27)	
	3	200	34	0	350	610	85	0.61 (±0.004)	1.14 (±0.69)	0.77 (±0.61)	2.51 (±0.10)*	
	6	400	70	0	370	750	90	1.07 (±0.35)	1.09 (±0.18)	0.98 (±0.33)	2.25 (±0.11)**	20
E	Pre			11	410	–	–	0.83 (±0.02)*,**	1.25 (±0.05)*	0.67 (±0.03)*	2.59 (±0.21)*	10
	1	25	13	11	400	–	–	1.04 (±0.004) *	1.12 (±0.17)	0.95 (±0.16)	3.18 (±0.18)**	
	3	75	25	11	250	–	–	1.16 (±0.08)**	1.31 (±0.05)**	0.88 (±0.03)*	4.27 (±1.00)***	
	6	100	34	18	410	–	–	0.57 (±0.13)	0.99 (±0.06)*,**	0.58 (±0.15)	0.68 (±0.35) *,**,***	11
F	Pre			10	3950	–	400	0.31 (±0.06)	0.25 (±0.08)*	1.29 (±0.19)	1.01 (±0.03)	76
	1	200	18	10	4200	–	400	1.02 (±0.07)	1.18 (±0.21)*	0.88 (±0.10)	1.37 (±0.39)	
	3	400	26	9	4290	–	420	1.64 (±0.91)	1.37 (±0.55)	1.15 (±0.25)	1.24 (±0.43)	79
G	Pre			1	400	1570	95	0.62 (±0.16)	1.13 (±0.16)	0,55 (±0.02)	1.12 (±0.11)*	19
	1	200	47	1	410	1440	95	0.66 (±0.15)	1.09 (±0.17)	0.60 (±0.08)	1.31 (±0.32)	
	3	400	50	1	410	1350	105	0.57 (±0.13)	1.44 (± 0.10)	0.40 (± 0.10)	0.73 (±0.01)*	
	6	400	43	1	420	1200	95	0.76 (±0.01)	1.65 (±0.78)	0.53 (±0.21)	1.77 (±0.02)*,**	18

All data for *SMN* transcription are expressed as the mean (±SD).

*,**,***$P < 0.05$. Tukey's or a Games–Howell *post-hoc* test was used to evaluate the differences in each level of *SMN* transcript or ratio of FL/Δ7-*SMN*in each patient.

CPF, cough peak flow; MIC, maximum insufflation capacity; VC, vital capacity.

Neurology and Clinical Neuroscience (2014) 1–9

the 6-month study, whereas case F was eliminated after 3 months because of chronic cholecystitis (no evident relationship to VPA trial).

VPA was started at 25–200 mg/day and gradually increased, with a final dosage in cases B, C, D and G of 400 mg/day, and 100 mg/day in case E, while the dose in case F at 3 months was 400 mg/day. VPA concentration reached an optimal range after 3 months in case C, and 6 months in case D. In cases B and G, the transient moderate VPA concentration was decreased under the optimal range at 6 months. In cases E and F, VPA concentration was at less than the optimal range during the study. Serum levels of VPA concentration in each patient are summarized in Table 2.

In cases A and B, L-carnitine was administered at 300 mg throughout the study. In case C, after starting L-carnitine at 300 mg, the dosage was decreased to 100 mg from the second week because of abdominal discomfort, and then increased to 200 mg from week 6. In case D, L-carnitine was started at100 mg and increased to 200 mg in week 5, then decreased to 100 mg in week 6 because of discomfort. In cases E and G, L-carnitine was administered at 100 mg throughout the study. In case F, L-carnitine was started at 100 mg and increased to 200 mg in week 5.

MHFMS, respiratory function and SMN transcript. Table 2 shows sequential changes in scores for MHFMS, respiratory function and transcription amount of *SMN* for each patient. Furthermore, Table 3 presents a summary of changes in MHFMS score, and rates of change in respiratory function and FL-*SMN* transcription from pretreatment to 6 months after beginning VPA administration in each case (3 months in case F).

MHFMS for cases C, D and G did not change during the dosage period (cases C and D: 0 points, case G: 1 point). MHFMS in case B was 4 points in a pretreatment evaluation and 5 points at 6 months later, while that in case F was 10 points at pretreatment and 9 points at 3 months. MHFMS in case E was 11 points at the pretreatment evaluation and increased to 18 points at 6 months. Case E gained motor function to turn from side to side.

There was a great number of improved respiratory function items even in cases with a VPA blood level lower than optimal, all of which were cases with progression. VC increased in cases C, F and G, while MIC increased in cases B, C and D, but decreased in case G, and CPF increased in cases C, D and F.

The transcription amount of FL-*SMN* generally showed an increasing tendency, whereas that of Δ7-*SMN* and total-*SMN*, and the ratio of FL/Δ7-*SMN* showed no consistent tendency in accordance with VPA administration in the patients. In some cases, the difference in level of *SMN* transcript or ratio of FL/Δ7-*SMN* was significant.

VPA concentration, MHFMS, respiratory function and transcription amount of FL-SMN in each case. Case B: VPA blood level after 6 months administration was lower than an optimal level. However, MIC increased and the FL-*SMN* transcription product quantity showed an increasing tendency.

Case C: VPA blood level was within an optimal level, whereas VC, MIC and CPF increased, and the quantity of the FL-*SMN* transcription product showed an increasing tendency.

Case D: VPA blood level was within an optimal level, whereas MIC and CPF increased. The quantity of the FL-*SMN* transcription product showed an increasing tendency.

Case E: MHFMS score was dramatically improved, as described earlier. However, VPA blood level at 6 months after administration was lower than optimal, and the quantity of the FL-*SMN* transcription product showed a decreasing tendency.

Case F: Although VPA blood level was lower than an optimal level and MHFMS worsened, VC and CPF increased, and the quantity of the FL-*SMN* transcription product showed an increasing tendency.

Case G: VPA blood level was lower than an optimal level and MIC decreased. There was no change in MHFMS, However, VC increased and the quantity of the FL-*SMN* transcription product showed an increasing tendency.

Subjective symptoms, side-effects and changes in bodyweight. Case A: Malaise, sleepiness and a precordial sense of incongruity.

Case B: Condition immutability and sleepiness.

Case C: Condition immutability and a precordial sense of incongruity.

Case D: Difficulty with fatigue and a precordial sense of incongruity.

Case E: Parents think that tremors have decreased.

Table 3 Summary of data obtained for each patient at end of administration of Valproic acid (6 months, 3 months for Case F). Valproic acid concentration, changes in Modified Hammersmith Functional Motor Scale for SMA, respiratory function and transcription amount of FL-*SMN*.

Case	VPA concentration	MHFMS	VC	MIC	CPF	FL-*SMN*
B	Below	1	−3.6	10.4	−7.1	Increasing tendency
C	Optimal	0	31.6	12.7	17.6	Increasing tendency
D	Optimal	0	−2.6	70.5	20	Increasing tendency
E	Below	7	0	-	-	Decreasing tendency
F	Below	−1	8.6	-	5	Increasing tendency
G	Below	0	5	−23.6	0	Increasing tendency

Data shown represent changes in score of Modified Hammersmith Functional Motor Scale for SMA (MHFMS), rate of change (%) in respiratory function from pretreatment to 6 months after administration of valproic acid (VPA) (3 months in case F).
CPF, cough peak flow; MIC, maximum insufflation capacity; VC, vital capacity.